AFRL-AFOSR-JP-TR-2018-0029

Plasmonic Optoelectronic Interactions (NBIT III)

Chad Mirkin
NORTHWESTERN UNIVERSITY

04/10/2018
Final Report

DISTRIBUTION A: Distribution approved for public release.

Air Force Research Laboratory
AF Office Of Scientific Research (AFOSR)/ IOA
Arlington, Virginia 22203
Air Force Materiel Command

REPORT DOCUMENTATION PAGE

Form Approved
OMB No. 0704-0188

The public reporting burden for this collection of information is estimated to average 1 hour per response, including the time for reviewing instructions, searching existing data sources, gathering and maintaining the data needed, and completing and reviewing the collection of information. Send comments regarding this burden estimate or any other aspect of this collection of information, including suggestions for reducing the burden, to Department of Defense, Executive Services, Directorate (0704-0188). Respondents should be aware that notwithstanding any other provision of law, no person shall be subject to any penalty for failing to comply with a collection of information if it does not display a currently valid OMB control number.
PLEASE DO NOT RETURN YOUR FORM TO THE ABOVE ORGANIZATION.

1. REPORT DATE *(DD-MM-YYYY)*	2. REPORT TYPE	3. DATES COVERED *(From - To)*
10-04-2018	Final	14 Aug 2013 to 13 Aug 2017

4. TITLE AND SUBTITLE
Plasmonic Optoelectronic Interactions (NBIT III)

5a. CONTRACT NUMBER

5b. GRANT NUMBER
FA2386-13-1-4124

5c. PROGRAM ELEMENT NUMBER
61102F

6. AUTHOR(S)
Chad Mirkin

5d. PROJECT NUMBER

5e. TASK NUMBER

5f. WORK UNIT NUMBER

7. PERFORMING ORGANIZATION NAME(S) AND ADDRESS(ES)
NORTHWESTERN UNIVERSITY
633 CLARK ST EVANSTON
EVANSTON, IL 60208-0001 US

8. PERFORMING ORGANIZATION REPORT NUMBER

9. SPONSORING/MONITORING AGENCY NAME(S) AND ADDRESS(ES)
AOARD
UNIT 45002
APO AP 96338-5002

10. SPONSOR/MONITOR'S ACRONYM(S)
AFRL/AFOSR IOA

11. SPONSOR/MONITOR'S REPORT NUMBER(S)
AFRL-AFOSR-JP-TR-2018-0029

12. DISTRIBUTION/AVAILABILITY STATEMENT
A DISTRIBUTION UNLIMITED: PB Public Release

13. SUPPLEMENTARY NOTES

14. ABSTRACT
During the past four years, the this team has successfully developed template-assisted syntheses that can be used to generate nanomaterials with new structures and compositions. In particular, the invention and development of on-wire lithography (OWL) and coaxial lithography (COAL) have enabled the syntheses of solution-dispersible nanowires with architectural control over both the axial and radial dimensions, such that core-shell semiconductor nanowireplasmonic nanoring structures - can be realized. In addition to electrochemical synthesis, the team also has reported a template-assisted solution-based process for the preparation of uniform nanostructured metal-halide perovskites. This class of materials has recently emerged as a promising material in photovoltaic, optoelectronic, and other energy harvesting devices.

15. SUBJECT TERMS
NBIT, Nanoscience, AOARD

16. SECURITY CLASSIFICATION OF:			17. LIMITATION OF ABSTRACT	18. NUMBER OF PAGES	19a. NAME OF RESPONSIBLE PERSON
a. REPORT	b. ABSTRACT	c. THIS PAGE			KNOPP, JEREMY
Unclassified	Unclassified	Unclassified	SAR	34	**19b. TELEPHONE NUMBER** *(Include area code)* 315-227-7006

Final Report for AOARD Grant
FA2386-13-1-4124

"Plasmonic Optoelectronic Interactions (NBIT III):

Hybrid plasmonic interaction: collective and spin-coupled plasmonic systems"

Professor Chad A. Mirkin: November 13, 2017

- e-mail address : chadnano@northwestern.edu
- Institution : Dept. of Chemistry, Northwestern University
- Mailing Address : 2145 Sheridan Rd, Evanston, IL 60208, USA
- Phone : +1-847-467-7302
- Fax : +1-847-467-5123

Professor Jae-Won Jang:

- e-mail address : jjang@pukyung.ac.kr, jjang@pknu.ac.kr
- Institution : Dept. of Physics, Pukyong National University
- Mailing Address : 45, Yongso-Ro, Nam-Gu, Busan 608-737, Rep. of Korea
- Phone : +82-51-629-5575
- Fax : +85-51-629-5549

Period of Performance: 08/14/2013 – 08/13/2017

Abstract:

During the past four years, the Mirkin Group has successfully developed template-assisted syntheses that can be used to generate nanomaterials with new structures and compositions. In particular, the invention and development of on-wire lithography (OWL) and coaxial lithography (COAL) have enabled the syntheses of solution-dispersible nanowires with architectural control over both the axial and radial dimensions, such that core-shell semiconductor nanowire–plasmonic nanoring structures - can be realized. In addition to electrochemical synthesis, the Mirkin group also has reported a template-assisted solution-based process for the preparation of uniform nanostructured metal-halide perovskites. This class of materials has recently emerged as a promising material in photovoltaic, optoelectronic, and other energy harvesting devices.

Also, based on expertise in nanoparticle assembly techniques using chemically modified oligonucleotides, the Mirkin group has realized plasmonic photonic crystals composed of inorganic nanoparticles uniformly arranged into crystalline lattices. In addition, fluorescent dye molecules also can be attached to the DNA to incorporate them into these plasmonic photonic crystals, where the collective effect of plasmon (nanoparticle) - exciton (dye) interactions can be studied. Moreover, the Mirkin group has continued to work with magnetic nanoparticles functionalized with oligonucleotides, assembling them into lattices even in conjunction with plasmonic nanoparticles as a means to realize yet-to-be-studied magnetically active colloidal crystals.

The Jang Group has continued to elucidate the mechanism of plasmonic photocurrent enhancement in semiconducting nanowire (NW) systems by metal nanoparticles (NPs), carrying out in-depth characterization utilizing advanced scanning probe microscopy. As a result, it was found that the energy band-matching between the metal NP and the semiconductor NW is important in determining the role of the metal NP as either an electron donor or accepter during plasmonic excitation. In the extended research period, wavelength-

DISTRIBUTION A. Approved for public release: distribution unlimited.

and spin alignment-dependent charge carrier transfer in ferromagnetic NWs with a plasmonic excitation structure (Au double rings) was investigated and demonstrated to show spin-coupled plasmonic phenomena. Importantly, this work is based upon the close collaboration of the Mirkin group (USA) and the Jang group (Korea) in which protocols, samples, and personnel have been extensively exchanged.

Introduction:

Compared to their bulk counterparts, nanomaterials are known to exhibit unique properties that can be exploited to fabricate optoelectronics devices that display enhanced performance. However, it is essential to understand light-matter interactions at the nanoscale and be able to synthesize novel (and complex) nanostructures, assemble them into well-defined arrays and probe their properties with high resolution. As a part of the NBIT collaborative research of the Mirkin and the Jang groups, light-matter interactions of different classes of materials (i.e., semiconducting, metallic, or magnetic) as well as their hybrid structures were investigated and this knowledge was applied to the fabrication of functional optoelectronic devices.

For the past decade, the Mirkin group has employed anodized aluminum oxide (AAO) templates to synthesize multicomponent nanowires within parallel and cylindrical nanopores, typically *via* electrochemical deposition. The library of materials that can be synthesized in this fashion include metals (e.g., Au, Ni, Ag, Pd), simple inorganic semiconductors (e.g., ZnO, MnO_2, CdS), and polymers (e.g., polypyrrole, polyaniline, polythiophene, their derivatives). During the earlier stage of the NBIT funding period, we reported a novel technique, termed coaxial lithography (COAL), which enables one to synthesize core-shell nanostructures. Briefly, post-deposition polymer contraction leaves a small gap between it and the pore wall and subsequent electrodeposition then occurs as a shell around the polymer core. As a result, COAL enables the synthesis of semiconducting nanowires surrounded by metallic nanorings, a type of plasmonic-optoelectronic hybrid structure, and solution-dispersible 2D cavity structures, complementing the 1D cavity structures synthesized by on-wire lithography (OWL).

Moreover, the porous AAO membranes have been utilized for fabricating nanostructured metal-halide perovskites, expanding the library of materials that can be prepared via template-assisted synthesis to those that can be cast from solution (i.e., spin-coating a precursor solution and evaporating the solvent). Over the past few years, metal halide perovskites (of which the most studied composition has been of the chemical formula $CH_3NH_3PbI_3$) have emerged as a promising class of low-cost, solution-processable semiconductors with highly desirable properties as components in photovoltaics (e.g., due to efficient visible light absorption and long charge diffusion lengths), LEDs, and lasers. Nanostructuring this perovskite material within AAO could offer benefits including improved crystallinity (compared to bulk films), reduced charge separation distances for more efficient charge extraction, and the unique opportunity to controllably interface perovskite nanowires with other functional materials (e.g., plasmonic nanorings).

The Mirkin group also used DNA-mediated nanoparticle assembly to realize the construction of plasmonic-semiconducting and plasmonic-magnetic hybrid nanostructures. Throughout the past decades, colloidal crystallization using surface-immobilized DNA has been advanced to generate single-crystalline superlattices of nanoparticle cores of different sizes, shapes, and compositions. The interparticle distances and lattice parameters are highly controllable in these structures, enabled by the rigidity of DNA, and optically functional molecules, such as fluorescent dyes can be incorporated at specific locations on a DNA strand using click chemistry. In these structures, unusual optical properties were observed that derive from the microscale geometries of the crystalline superlattices and the strong

DISTRIBUTION A. Approved for public release: distribution unlimited.

interactions between the plasmonic and excitonic components.

In parallel to the development of the synthetic platform by the Mirkin Group, the Jang group focused on the characterization and nanoscale visualization of the effect of the plasmonic optoelectronic interactions. In addition to the previously reported measurement schemes, light-irradiated Kelvin Probe Force Microscopy (KPFM) was introduced to the library of analytical tools that could be used to probe nanostructures. Systematic control over nanostructured metal/semiconductor junctions enables one to access an ideal testbed to explore light-matter interactions. As a complementary investigation of the light-matter interactions of COAL-based nanowires, metal nanoparticles (NPs) coordinated to semiconductor NW devices have been used for a plasmonically enhanced photocurrent study. We previously reported that Au NPs attached to p-type polypyrrole NWs cause plasmonic enhancement of photocurrent generation, and we employed light-irradiated KPFM to inform the mechanism by which this enhancement occurs. In addition to magnetic force microscopy (MFM), light-irradiated KPFM has been used as a tool to characterize spin-coupled plasmonic interactions in Fe NWs with plasmonic Au double ring structures. We propose that the metal NP can work as either an electron donor or acceptor depending on the type of semiconductor NW (p-type or n-type) using light-irradiated KPFM with Au NPs attached to PPy NWs. In case of spin-coupled plasmonic interactions, the surface potential difference as a result of the plasmonic excitation in the Fe NWs with Au rings is relatively large when the external field-aligned magnetic moment of the Fe NW is perpendicular to the electrical component of the applied light. Our demonstration reveals that the bandgap-matching of the metal and the semiconductor is important for determining the direction of the electron movement in the nanostructured metal/semiconductor junction.

It is worth emphasizing that while the synthetic work was primarily done by the Mirkin group, the architectures of interest were chosen through close collaboration with the Jang group. We have leveraged the collaboration formalized by this grant to characterize the properties of the wires utilizing the advanced optoelectronic measurement set-up constructed by the Jang group, including light-irradiated KPFM and MFM. These coordinated optical and electrical measurements are a powerful and necessary part of realizing new architectures for studying light-matter interactions as well as investigating spin-coupled plasmonic interactions.

Experiment:

1. Synthetic advances through template-assisted synthesis (Mirkin group)

As mentioned briefly above, coaxial lithography (COAL) is a technique by which core-shell nanowires can be synthesized in a high-throughput manner with sub-10 nm resolution, and compositional control in both the axial and radial dimensions. This method is enabled by polymer electrodeposition (polyaniline was often used in this study); the polymer contracts inside the pores when it dries after deposition. Then, through the small gap between the polymer core and the AAO pore wall, further deposition can be performed to grow multi-segmented shell layers, composed of, for example, Au or Ni, around the core (**Figure 1**). It is noteworthy that the metal segments or the polymer core can be selectively removed, and based on this, many variations of the structure can be made.

DISTRIBUTION A. Approved for public release: distribution unlimited.

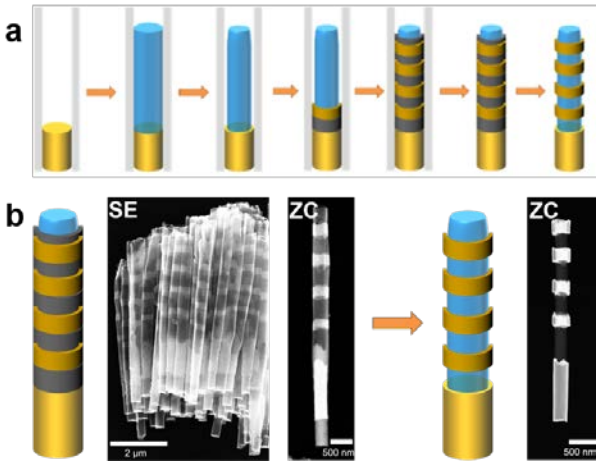

Figure 1. (a) General scheme showing the synthesis of metal nanorings around an organic core. Blue: organic core. Yellow: target material (Au). Grey: sacrificial material (Ni). On top of the first Au segment, polymer is deposited that subsequently shrinks when exposed to vacuum. Around the polymer core, the shell layers can be deposited from the bottom. (b) STEM images in secondary electrons (SE) and z-contrast (ZC) modes show typical NWs before (left) and after etching (right) the sacrificial Ni shell to generate Au rings (outer diameter: 340 nm) around a polypyrrole (PPy) core (diameter: 280 nm).

An example would be the generation of solution-dispersible nanorings made of various metals with tailorable dimensions (**Figure 2**). Here, before the deposition of the shell layers (i.e., nanorings), the template and the polymer core can be carefully etched using the appropriate etchants: the AAO template can be dissolved using 0.5 M NaOH and the polyaniline core can be slowly dissolved using a mixture of ethanol and water, allowing for precise control over the outer and the inner diameters, respectively, of the final ring structure. Also, the height of the rings can be controlled as a function of the amount of charge passed during the electrochemical deposition of the shell layers. Then, following the steps to completely remove the AAO template (3 M NaOH), polyaniline core (acetone), and sacrificial metal layers (respective oxidants), the nanorings can be released into solution. By tailoring the dimensions and compositions, the localized surface plasmon resonance (LSPR) of the nanorings can be controlled (**Figure 2**). The fabrication of single nanowire-based optoelectronic devices with plasmonic nanorings also was demonstrated. As mentioned, the polymer core (polyaniline) and sacrificial Ni segments can be selectively removed, leaving Au nanorings in the pores of the template. Then, semiconducting materials (e.g., MnO_2 or CdSe) are electrochemically deposited in the core (**Figure 3**).

DISTRIBUTION A. Approved for public release: distribution unlimited.

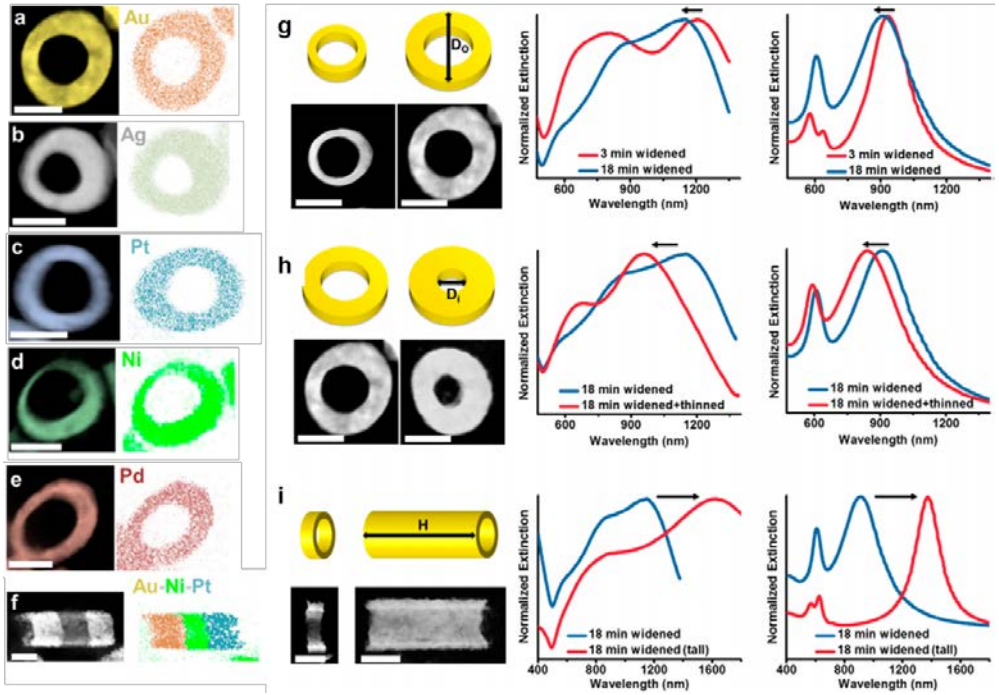

Figure 2. Characterization of nanorings composed of different materials. STEM images (left) and elemental maps via energy-dispersive X-ray spectroscopy (EDS, right) of single component (a) Au, (b) Ag, (c) Pt, (d) Ni, and (e) Pd nanorings and a multicomponent (f) Au−Ni−Pt nanotube. STEM images in (a), (c), (d), and (e) are false-colored to match the EDS color mapping. (g-i) Control over all three architectural parameters of Au nanorings. STEM images (left), measured extinction spectra (middle), and calculated extinction spectra (right) of the nanorings are presented. (g) The outer diameter was enlarged from 156 to 179 nm by increasing the duration of the pore-widening step from 3 to 18 min (maintaining constant inner diameter and aspect ratio), which corresponds to a 50 nm blue-shift in the most intense LSPR wavelength. (h) The inner diameter was reduced from 95 to 64 nm (maintaining constant outer diameter and aspect ratio) through the introduction of the polymer-thinning step; this corresponds to a 192 nm blue-shift in the LSPR wavelength. (i) The height was increased with the amount of charge passed through the electrodes during the electrodeposition step. By increasing the applied charge from 350 to 1750 mC, the aspect ratio was increased from ~0.4 to ~1.8 (maintaining constant outer and inner diameters), which corresponds to a significant red-shift in the lowest frequency plasmon resonance wavelength by 478 nm. Scale bars are 100 nm in all of the electron microscopy images. The blue curves in all of the extinction spectra correspond to the control nanoring sample.

DISTRIBUTION A. Approved for public release: distribution unlimited.

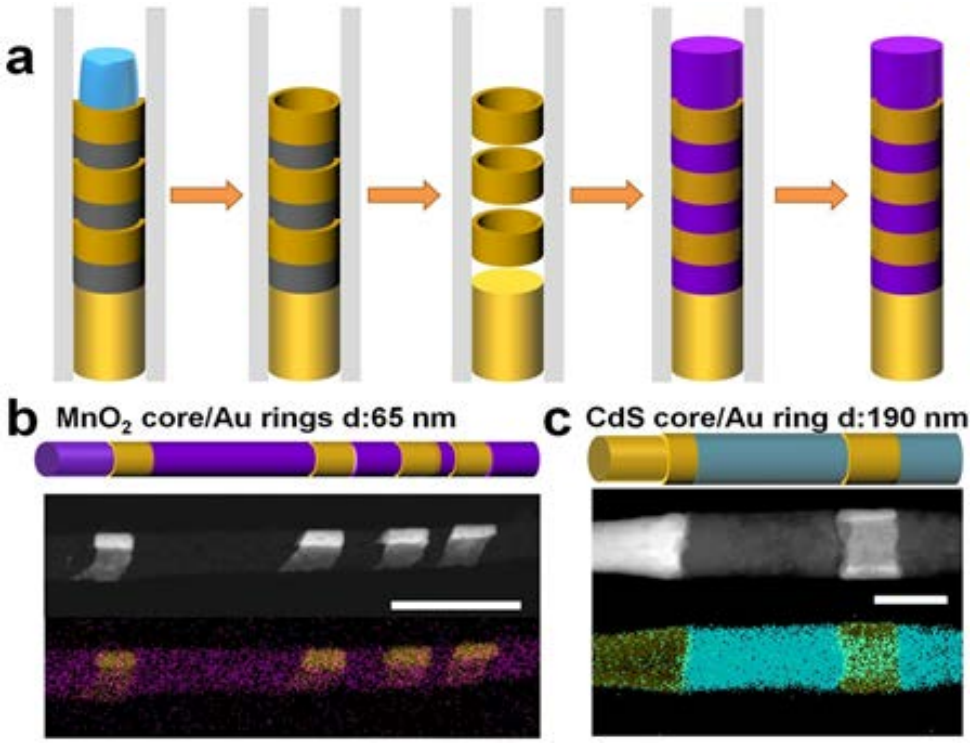

Figure 3. Generalization of COAL to inorganic core materials. (a) Scheme illustrating the modified synthetic steps. From left to right: dissolution of the PANI core (shown in blue), etching of the sacrificial segments (grey) within the AAO template, deposition of the new core material (purple), dissolution of the AAO template. ZC STEM images and elemental map of: (b) multiple Au rings (inner diameter: 55 nm) around a MnO_2 core (MnO_2 diameter: 65 nm; elemental map: yellow corresponds to Au and purple to Mn), (c) single Au ring (inner diameter: 140 nm) around a CdS core (CdS diameter: 190 nm; elemental map: yellow corresponds to Au and blue corresponds to Cd). Scale bars: 200 nm.

As a demonstration for how COAL-synthesized structures can be used to study light-matter interactions, the Mirkin group synthesized nanoring-embedded hybrid core-shell semiconductor NWs. The target architecture consisted of a p-type semiconducting core surrounded by a Au ring at a deliberately programmed location. This entire structure was surrounded by a n-type semiconducting shell with pure Au segments affixed to either end of the wire. This novel NW architecture was not only chosen for its complexity, but also because it should enhance the absorption of visible light without significantly blocking the electron-hole flow through the wire. COAL was used to initially make Ni and Au rings around a polymeric core (polyaniline, **Figure 1**). Then, the polymer was dissolved with acetone, and the Ni segment was etched with aqueous 3% $FeCl_3$ to generate a Au ring within the pores at a deliberately chosen location (**Figure 4a**). P-type poly(3-hexylthiophene) (P3HT) was then polymerized within the pores, and the pores were subsequently widened by slow dissolution with aqueous 0.5 M NaOH. The n-type semiconductor (CdSe) was then electrochemically deposited to surround the ring-encased p-type semiconductor. At the end of this wire, a Au segment was electrodeposited as an electrical contact to generate the target device architecture. A z-contrast image of a typical NW consisting of a P3HT core (diameter: 120 nm) surrounded by a 175-nm wide, 75-nm long Au ring, further encased in CdSe (outer diameter: 235 nm) clearly shows that all components are where they were programmed to be (**Figure 4b**).

DISTRIBUTION A. Approved for public release: distribution unlimited.

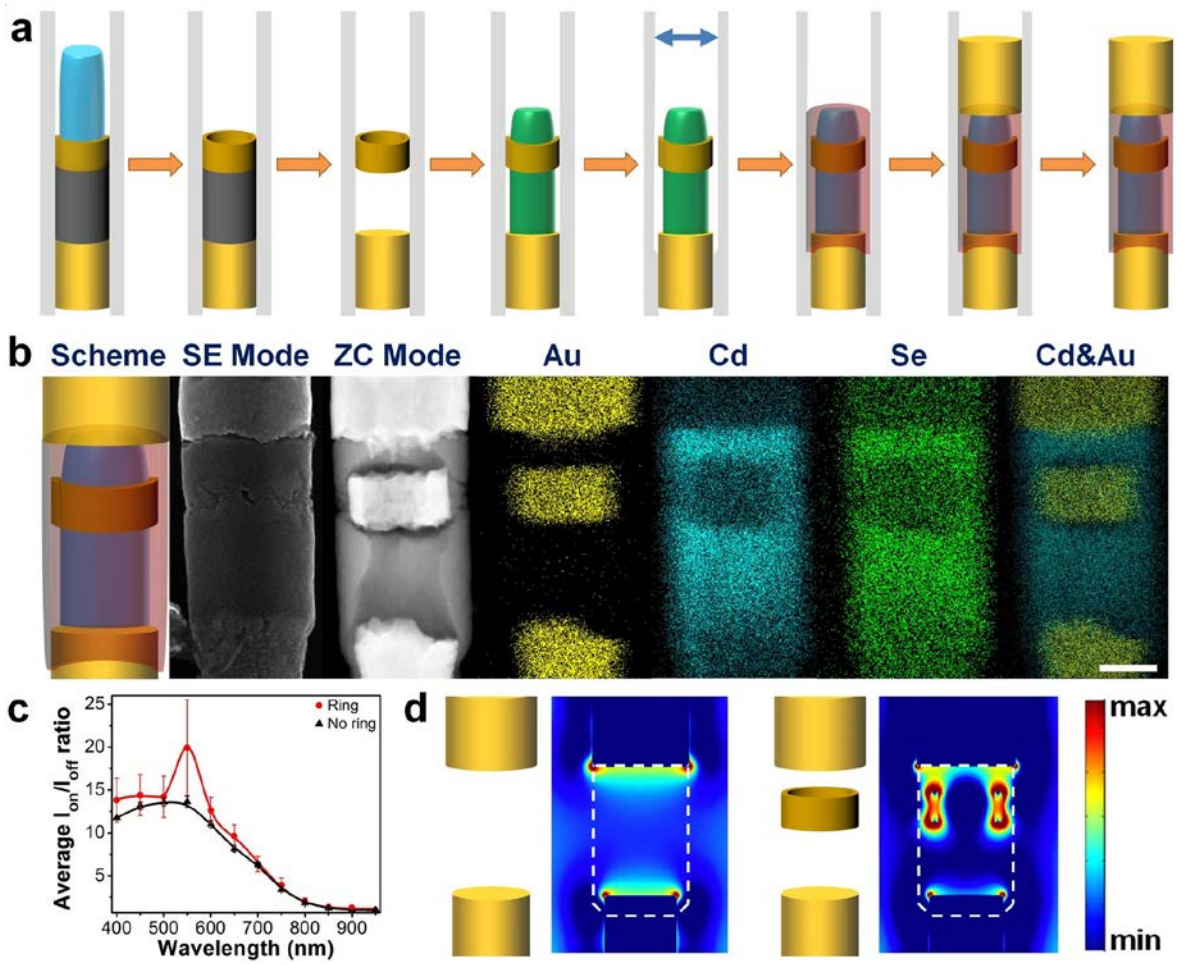

Figure 4. Integration of a plasmonic Au ring within a hybrid junction composed of an organic p-type core (P3HT) and an inorganic n-type shell (CdSe). (a) Scheme illustrating the modified synthesis steps. From left to right: dissolution of the PANI core (shown in blue), etching of the sacrificial segments (grey) within the AAO template, deposition of the P3HT core (green), pore widening step, growth of the CdSe shell (red) around the P3HT core and the Au ring (yellow), deposition of the top Au segment and dissolution of the AAO template. (b) SE and ZC STEM images, and elemental maps of the P3HT core/CdSe shell NWs with a Au ring (yellow: Au, blue: Cd, and green: Se). Scale bars are 100 nm for all of the images. (c) Comparison of the average I_{on}/I_{off} ratios as a function of wavelength of the NWs with (red circles) and without a ring (black triangles). Three NWs were measured in each case (with and without a ring). The error bars correspond to the standard errors of the experimental measurements. The red and black lines are only guides for the eye. (d) Simulated electric-field intensity maps of the metal segments (NW shown in b), without (left) and with (right) a ring, recorded at 532 nm (logarithmic scale). The maps were generated using an excitation source polarized in the direction parallel to the longitudinal axis of the NWs. The dotted line corresponds to the location of the semiconductor segments.

The effect of the embedded plasmonic ring on the photoconducting properties of the core/shell NW was investigated by performing electrical measurements under vacuum. NWs made in this manner and similar structures without Au rings were irradiated using a Xe lamp with a monochromator while the I-V characteristics were measured (**Figure 4c**). The plasmonic nanoring was found to modify the photoresponse of the NWs as evidenced by the rise in photocurrent at the LSPR wavelength of the Au ring (**Figure 4d**). Indeed, I_{on}/I_{off} at this wavelength was on average 45% higher than for structures without the Au rings (3 wires averaged for each condition). FDTD simulations suggest that this enhancement arises from the greatly increased electric field within and around the Au ring at 532 nm (for simplicity, the semiconductor segment was not included in the model; however, a red shift is expected

DISTRIBUTION A. Approved for public release: distribution unlimited.

due to the higher dielectric constants of the semiconductors compared with vacuum).

The generation of vertically aligned perovskite ($CH_3NH_3PbI_3$) nanowires with controlled diameters have been demonstrated. To form $CH_3NH_3PbI_3$ nanowires in these templates, a $CH_3NH_3PbI_3$ precursor solution in dimethylformamide (DMF) was added and allowed to penetrate the pores of the AAO, followed by a removal of excess liquid from the template surface *via* spin-coating and annealing (**Figure 5a, I**). While this step results in crystalline perovskite nanowires, solvent evaporation from the AAO surface during annealing led to material contraction such that much of the perovskite material within the template did not touch the bottoms of the pores. In addition, a thin perovskite film remained on the surface of the AAO. To address these synthetic issues, we employed a surface-cleaning step, where a syringe pump dispensed a solution of dimethyl sulfoxide (DMSO) and chlorobenzene on the top of a rapidly rotating AAO template (**Figure 5a, II**). This solvent mixture dissolved the perovskite (as evidenced by a color change from dark red to transparent), removed residual material from the AAO surface, and drew liquid into the pores *via* capillary and centrifugal forces. Subsequent annealing led to perovskite recrystallization (as evidenced by the return to a dark red color) and nanowire formation at the bottoms of the pores. In this process, the high surface area at the pore bottoms relative to the pore walls likely favors preferential nucleation and materials growth at these locations, contributing to the formation of $CH_3NH_3PbI_3$ nanowires that conform to the cylindrical shape of the AAO pores. Importantly, this synthetic procedure can be used to generate large-area nanowire arrays (**Figure 5b**) over 75 cm^2 with uniform nanowires across the sample.

To test whether this procedure is amenable to size control, templates with different pore diameters were prepared. Indeed, $CH_3NH_3PbI_3$ nanowires with diameters (*D*) ranging from 50 - 200 nm (**Figure 5c-g**) can be easily synthesized. Importantly, the dispersity in D was <10% for most samples, as measured by SEM.

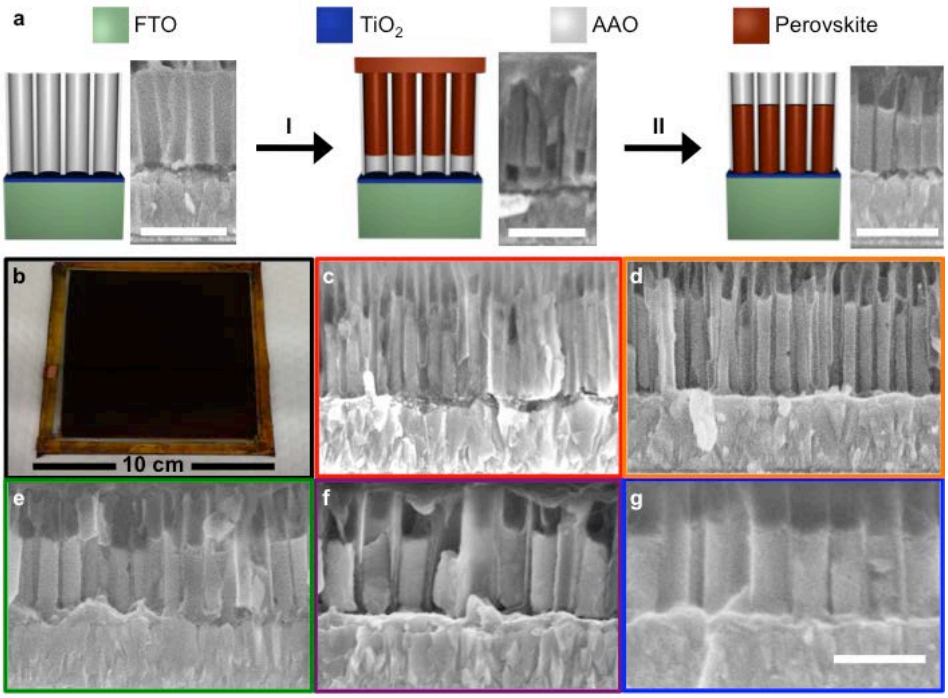

Figure 5. Synthesis of perovskite nanowire arrays in AAO. (a) A $CH_3NH_3PbI_3$ precursor solution penetrates the AAO pores, followed by spin coating and annealing (I); the sample is exposed to a DMSO:chlorobenzene solution followed by a short annealing step (II). (b) Photograph of a ~9 x 9 cm nanowire array. Cross-section SEM images of nanowires with diameters of (c) 50.3 ± 6.5 nm, (d) 70.0 ± 6.8 nm, (e) 107 ± 9.4 nm, (f) 155 ± 13 nm, and (g) 199 ± 19 nm. Nanowire lengths are consistently ~425 nm. Scale bars are 500 nm.

DISTRIBUTION A. Approved for public release: distribution unlimited.

2. DNA-mediated assembly of nanoparticles (Mirkin group)

The colloidal crystallization of DNA-modified nanoparticles has been heavily investigated by the Mirkin group and others. More than 500 colloidal crystals in ~40 different lattice symmetries have been realized via DNA-mediated crystallization. When identical nanoparticles are functionalized with two types of DNA that are complementary to each other, they form body-centered cubic (bcc) symmetries, and by a slow cooling crystallization process, these superlattices can grow into microscale rhombic dodecahedral single crystals (Wulff shape of bcc, **Figure 6a**). As part of the NBIT program, the optical properties of these faceted colloidal crystals have been studied, where strong light-plasmon interactions were observed. Significantly, modes at two different length-scales exist within a single crystal. At the micron-scale, Fabry-Perot type photonic modes exist, which can be tuned by controlling the size and shape of NP, and the volume fraction of the crystal. On the nano-scale, plasmonic modes are produced by individual nanoparticle building blocks and can be controlled by the nanoparticle size, shape, and composition. The two types of modes interact strongly with each other, giving rise to a polaritonic band gap (**Figures 6c and d-f**), which opens the door to studying exciton-photon coupling in novel photonic plasmonic cavities and exploring new directions in cavity QEDs, quantum optics, and quantum many-body dynamics.

In order to make use of this unique class of metamaterials and illustrate its potential as a novel cavity, excitonic elements can be added into the crystals. Alexa fluor dye molecules can be attached onto the DNA strand by incorporating amino modifier C6 dT at any designated position of the DNA sequence (**Figure 7**, d1, d2, and/or d3). Each DNA can contain either one dye or multiple dyes. For our initial investigation, only one dye was attached to each DNA strand. The process of attaching fluorophore-labeled DNA onto the NPs and assembling fluorophore-DNA-coated NPs into superlattices can be performed in the same way as when using DNA strands without dye molecules. With this technique, the distance between the dye molecules and the nanoparticle can be tuned with sub-nanometer precision, allowing for the systematic study the interaction between the photonic, plasmonic, and excitonic modes.

DISTRIBUTION A. Approved for public release: distribution unlimited.

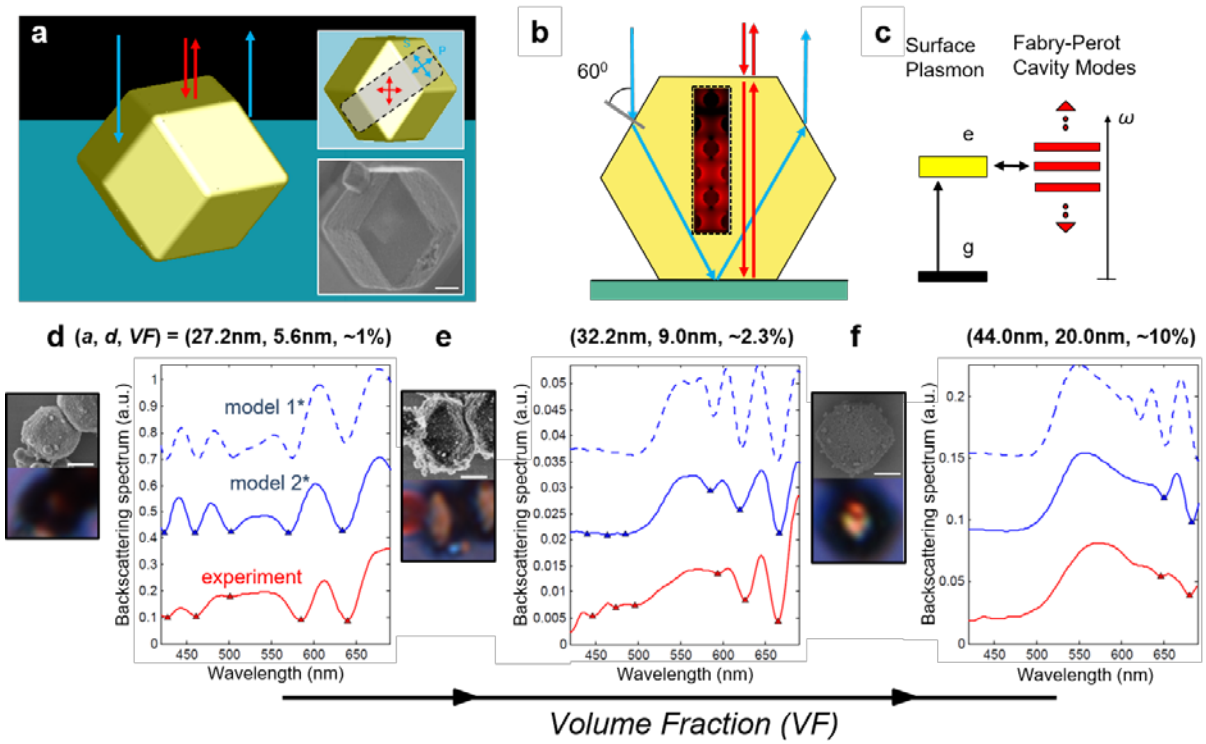

Figure 6. A polaritonic photonic crystal (PPC) made by DNA-programmable assembly. (a) Three-dimensional illustration of a plasmonic PPC, in the shape of a rhombic dodecahedron, assembled from DNA-modified gold nanoparticles. Red arrows indicate light rays normal to the underlying substrate, impinging on and backscattering through a top facet of the crystal (Febry-Perot cavity modes, FPMs). The blue arrows represent light rays entering through the slanted side facets and leaving the PPC through the opposite side, not contributing to the FPMs. The top right inset shows the top view of the crystal with two sets of arrows defining two polarization bases at the top and side facets. The bottom right inset shows an SEM image of a representative single crystal corresponding to the orientation of the top right inset. (Scale bar, 1 μm.) (b) A 2D scheme showing the geometric optics approximation of backscattering consistent with the explanation in (a). The hexagon outline is a vertical cross-section through the gray area in the top right inset of (a) parallel to its long edge. The box enclosed by a dashed line depicts the interaction between localized surface plasmons and photonic modes (red arrows; FPMs) with a typical near-field profile around gold nanoparticles. The contribution of backscattering through the side facets (blue arrows) to FPMs is negligible. (c) Schematic energy diagram for plasmon polariton formation. The localized surface plasmons (yellow bar) strongly couple to the photonic modes (red bars; FPMs). (d-f) Experimental and theoretical backscattering spectra of PPC1–3, having different volume fraction of Au. (d) SEM image (top left) and optical bright field reflection mode image (bottom left) of PPC1 on a silicon substrate. (Scale bar, 1 μm.) On the right, measured backscattering spectrum (red solid line) of PPC1 from the center red spot in the optical micrograph. Calculated backscattering spectra are based on two infinite slab models with BCC crystal geometry (blue solid line) and EMT approximation (blue dashed line). FPMs are indicated by markers. (e,f) The corresponding datasets for PPC2 and PPC3 as in (d). The optical images show bright spots at the center owing to backscattering from the top and bottom facets. All scale bars are 1 μm.

DISTRIBUTION A. Approved for public release: distribution unlimited.

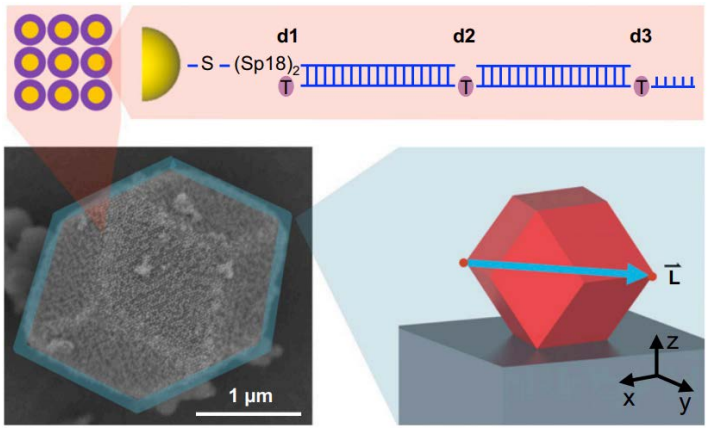

Figure 7. Scheme showing the 3D microcavity geometry (blue, Bottom Right) and a dye-coupled gold nanoparticle (magenta, Top) of dye-functionalized singlecrystal bcc superlattices. An SEM image shows a representative superlattice (Bottom Left). The superlattice is drop-cast onto a glass substrate leading to a facet facing up orientation (Bottom Right). Its RD shape can lead to 3D microcavity properties. L is defined as a vector connecting two vertices (two red dots) with the largest intervertex distance (blue arrow aligned with y axis, Bottom Right). Three L s can be defined in an RD, and they all pass through the center of the structure. The gold nanoparticles at the lattice sites in the superlattice (Top) are surrounded by multiple dye molecules forming a layer, and the distance between the gold surface and the dye layer is controlled by selecting a dye binding site among three sites (purple circles; denoted d1, d2, and d3 from left to right) on DNA strands. The dye molecules are chosen based on the spectral positions of their emission with respect to that of the surface plasmons, depending on the intended use.

3. Light-irradiated Kelvin probe force microscope (KPFM) (Jang group)

KPFM has been developed to monitor the surface charge state of sample. In KPFM (**Figure 8**) (reference: Lee et al. *Surface Science Reports* 66 (2011), 1-27), a conducting cantilever is scanned over a surface at a constant height to map the work function of the surface. When a tip-probe contacts the sample surface, a potential difference (V_{CPD}) is generated owing to difference between the work functions of the sample and KPFM tip-probe. V_{CPD} can be detected by applying bias (V_{DC}) to the tip-probe using a lock-in amplifier (**Figure 8b**). V_{CPD} decreases when the work function of the sample increases (with in-letting electrons). Hence, the change of the surface charge state of sample is sensitively measured by KPFM.

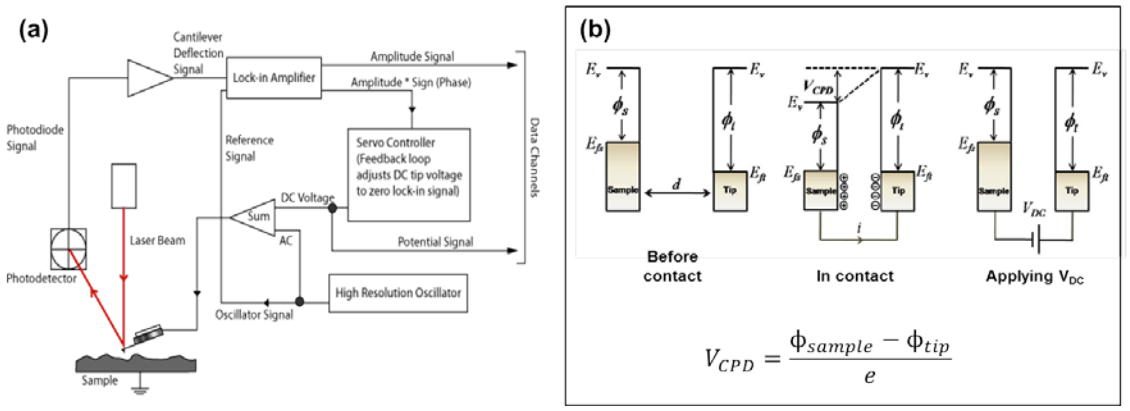

Figure 8. (a) Scheme of Kelvin probe force microscopy (KPFM) and (b) energy band diagram during KPFM measurement. The difference between the work functions of sample and tip is represented as V_{CPD}, which can be detected by applying bias (V_{DC}) to the tip-probe.

DISTRIBUTION A. Approved for public release: distribution unlimited.

Plasmonic excitation will change the surface charge state of sample, and it can be measured by KPFM. Therefore, we set-up a light-irradiated KPFM system (**Figure 9**). An additional light source, such as a wavelength tunable laser, is implemented to a KPFM spectrometer. One can observe the change of the surface charge state due to the plasmonic excitation of sample by varying the irradiated light wavelength. Therefore, the wavelength-dependent surface charge state of sample (i.e., plasmonic excitation) can be monitored with nanoscale spatial resolution. The light-irradiated KPFM system was established with introducing blue (λ = 450 nm), green (λ = 550 nm), and red (λ = 620 nm) lasers (500 mW) to a multimode atomic force microscope (Dimension ICON, Bruker Inc.). The blue light irradiated KPFM we are using is displayed in **Figure 9b**.

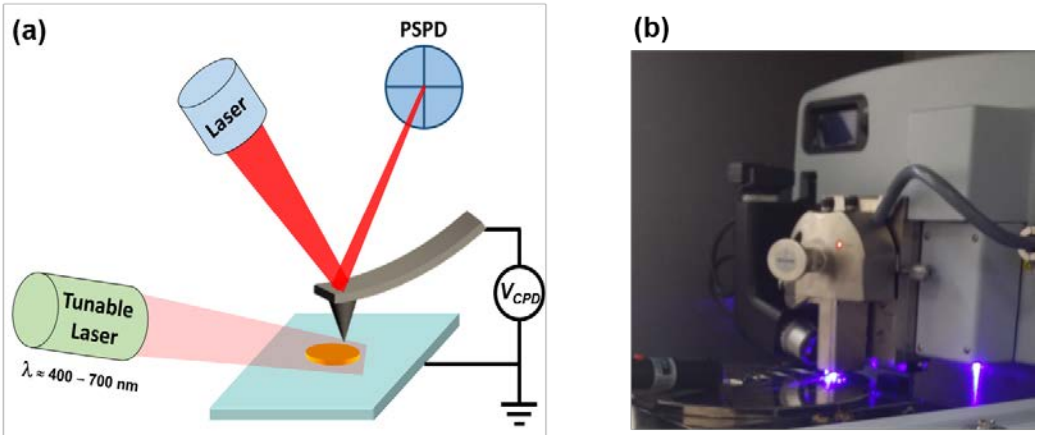

Figure 9. (a) Schematic diagram of light-irradiated KPFM. V_{CPD} is monitored at the same time with wavelength tunable light irradiation to the sample. (b) A snap shot image of light irradiated KPFM; KPFM measurement is being carried out under irradiation by a blue laser.

4. Plasmonic nanoparticle-decorated semiconducting nanowires (Jang group)

Ferromagnetic NWs with plasmonic structures have been fabricated by changing the core materials during COAL. After formation of Au ring structures during COAL, core materials can be chosen to be ferromagnetic. Fe has been deposited inside the empty holes of the AAO, where the Au rings are stuck on the walls inside the holes of the AAO; hence, ferromagnetic NWs decorated by plasmonic structures (Au double rings) were obtained (**Figure 10a)**. Energy-dispersive X-ray spectroscopy (EDS) mapping of the plasmonic structure (the boxed area of **Figure 10a**) is displayed as an inset and indicates that a Au double-ring structure has been prepared. To control the magnetic moment of the ferromagnetic part of the NW, Fe NWs with Au double rings were drop-dispersed on a substrate with markers (to note the orientation of the NWs). Two directional alignments of the magnetic moments, parallel and perpendicular directions corresponding to the NW axis, are established as shown in **Figure 10b**. As the next step, the magnetic moment aligned Fe NWs with Au double rings has been characterized by light-irradiated KPFM and MFM for investigating spin-coupled plasmon excitation.

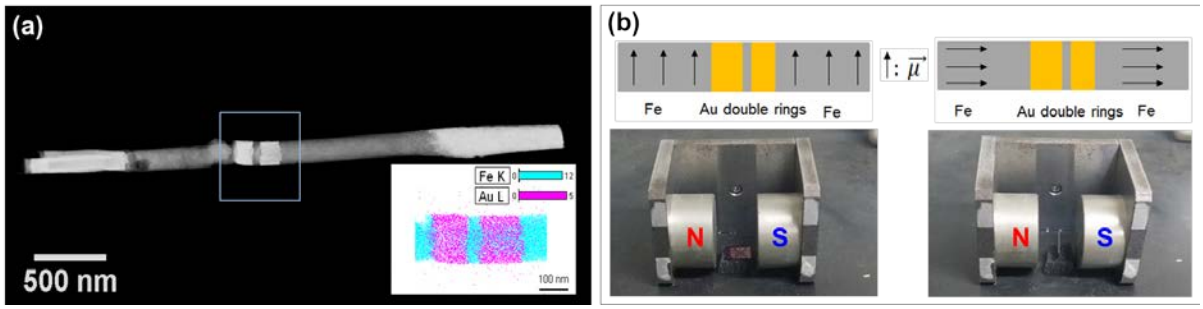

Figure 10. (a) High resolution SEM image and EDS mapping image (inset) of ferromagnetic NW with plasmonic structure. The box denotes where EDS mapping is carried out. (b) Schemes and snapshot images of aligning the magnetic moment of the Fe NWs with Au double ring structure.

Results and Discussion:

1. Template-assisted synthesis of perovskite nanowires (Mirkin group)

To better understand the effect of nanowire diameter on crystallinity, each sample was characterized by X-ray diffraction (XRD). These measurements confirmed that the target perovskite crystal structure was achieved for each of the nanowire samples (**Figure 11**). Subsequently, Williamson-Hall (WH) analysis was used to evaluate the relative crystallinity of each sample. This analysis separates the contributions of lattice strain (ε_{WH}) and crystallite size to peak breadth. To perform this analysis, the full-width at half maximum of five diffraction peaks characteristic of the $CH_3NH_3PbI_3$ perovskite crystal were plotted versus the diffraction angle (θ). For each sample, the data fit well to a linear model, as expected. Interestingly, D = 110 nm nanowires reproducibly exhibited the smallest absolute ε_{WH}, with greater ε_{WH} at both larger and smaller D (**Figure 12a**). This property is consistent with reduced defect density, which is directly related to the rate of charge recombination.

In order to elucidate structure-function relationships in perovskite nanowires, time-resolved photoluminescence spectroscopy experiments were performed to analyze charge transport dynamics. Decay curves were fit to a biexponential function, such that two distinct populations of excited charge carriers (i.e., those that undergo fast surface recombination *vs.* slow bulk recombination) could be described. For this comparative study, we report the overall characteristic lifetime (τ_c, which accounts for both populations of charge carriers) as a concise metric to evaluate charge transport within each nanowire sample (**Figure 12b,c**). As expected from WH analysis, D = 110 nm exhibited the longest τ_c (~60 ns), with reductions in τ_c observed with both increased and decreased D. The correlation between ε_{WH} and τ_c suggests that charge carrier lifetime is largely controlled by defect-driven lattice strain in these experiments.

DISTRIBUTION A. Approved for public release: distribution unlimited.

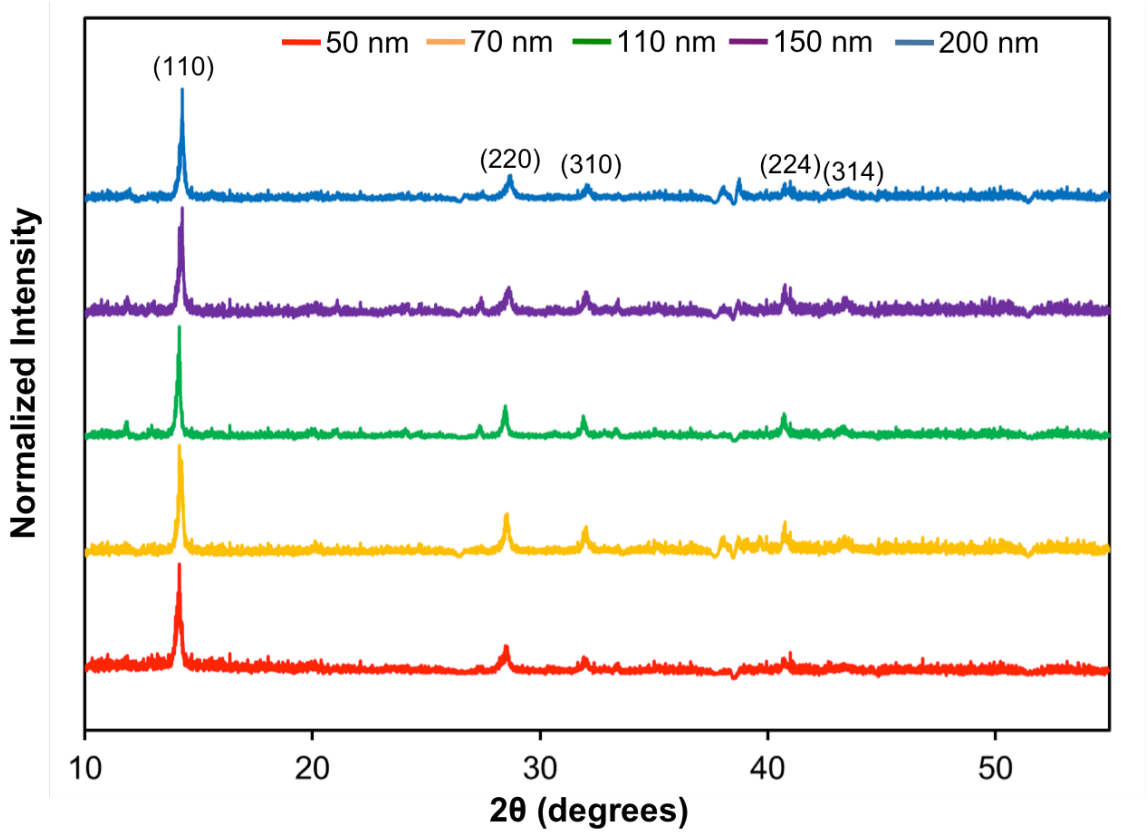

Figure 11. Representative powder XRD patterns of $CH_3NH_3PbI_3$ nanowires of controlled diameter. Five peaks characteristic to the $CH_3NH_3PbI_3$ perovskite crystal (space group: *I4/mcm*) are noted above the pattern for 200 nm nanowires (blue trace), which are consistent among each sample. The full-width at half maximum values of these peaks are subsequently used for Williamson-Hall analysis.

DISTRIBUTION A. Approved for public release: distribution unlimited.

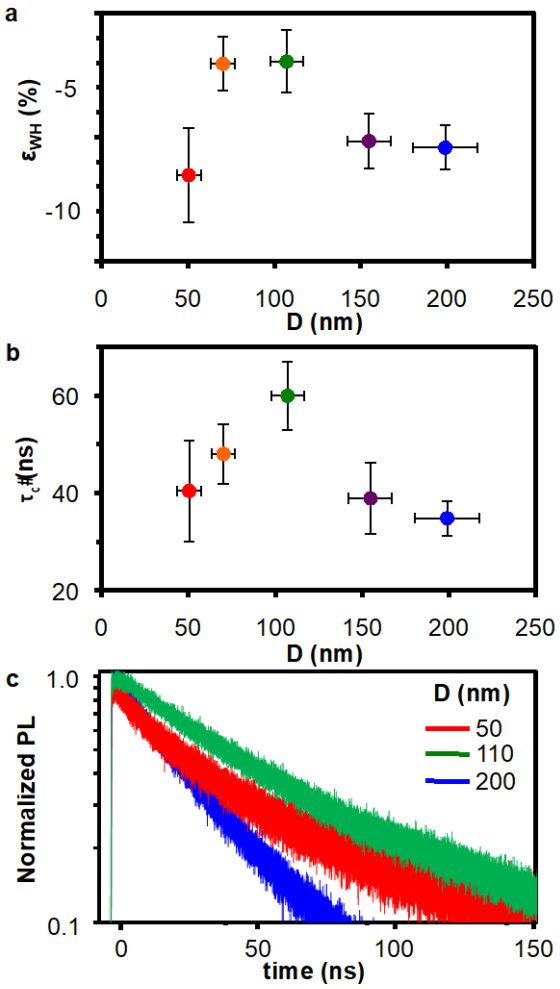

Figure 12. Structure-function relationships in $CH_3NH_3PbI_3$ nanowire arrays. (a) Estimated strain from WH analysis for different nanowire diameters (negative values signify lattice contraction). (b) Average τ_c for different nanowire diameters. (c) Representative PL decay curves.

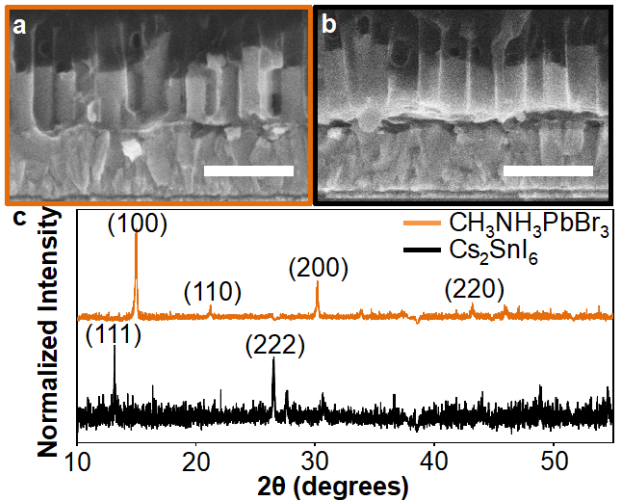

Figure 13. Compositional generality in the templated synthesis of perovskite nanowires. Cross-section SEM images of (a) $CH_3NH_3PbBr_3$ and (b) Cs_2SnI_6 nanowires. Scale bars are 500 nm. (c) Powder XRD patterns of $CH_3NH_3PbBr_3$ and Cs_2SnI_6 nanowires.

DISTRIBUTION A. Approved for public release: distribution unlimited.

In order to demonstrate the general nature of this approach, perovskite nanowires with a variety of compositions were synthesized. In particular, halide substitution is known to enable bandgap tunability in organolead halide perovskites (~1.55 – 2.3 eV). Use of the appropriate precursor solution and surface cleaning conditions indeed led to $CH_3NH_3PbBr_3$ nanowires with similar uniformity (**Figure 13a**). Beyond organolead halide perovskites, Cs_2SnI_6 has been investigated more recently as an inorganic, air-stable, lead-free alternative. After the synthesis of Cs_2SnI_6 powder, an analogous method was employed to deposit Cs_2SnI_6 nanowires from a single precursor solution (**Figure 13b**). XRD confirmed the expected crystal structures for both $CH_3NH_3PbBr_3$ and Cs_2SnI_6 nanowires (**Figure 13c**), and to the best of our knowledge, Cs_2SnI_6 nanostructures have not yet been synthesized using any other method.

The work presented here describes a new method for the synthesis of composition general perovskite nanowires with controlled diameter. The substrates used for synthesis (TiO_2/ fluorine-doped tin oxide (FTO)-bound AAO) should enable a facile transition from fundamental nanowire characterization to array photovoltaic device fabrication, as TiO_2, FTO, and AAO can act as a hole-blocking layer, transparent anode, and stabilizing scaffold, respectively, in an operational device. Moreover, the use of AAO in this way provides a unique opportunity to exploit the established synthetic abilities of the Mirkin Group. Specifically, the use of coaxial lithography (COAL) enables the synthesis of shell structures (i.e., rings and tubes) around nanowires with controlled placement and dimensions. We will employ COAL methodology to precisely place plasmonic Au nanorings around functional nanowires (i.e., semiconducting, magnetic; **Figure 14a,b**) in order to systematically elucidate the effects of plasmonic nanostructures on their optical, electronic, or magnetic properties. Importantly, core-shell nanowire constructs will be connected in parallel as an array; bulk electronic measurements can then be made *via* contact with the FTO substrate. Indeed, COAL can be executed within thin AAO templates, in which metallic segments (e.g., Ni and Au) can be electrodeposited around a contracted polyaniline core (**Figure 14c**). Subsequent dissolution of sacrificial segments followed by deposition of the desired nanowire material will enable the synthesis and testing of plasmon-enhanced semiconducting (i.e., photovoltaic) and magnetic nanowire array devices. Future work will focus on the optimization of these syntheses and device testing in which nanowire diameter and nanoring dimensions (outer diameter, inner diameter, and height) and position along the nanowire are systematically varied.

DISTRIBUTION A. Approved for public release: distribution unlimited.

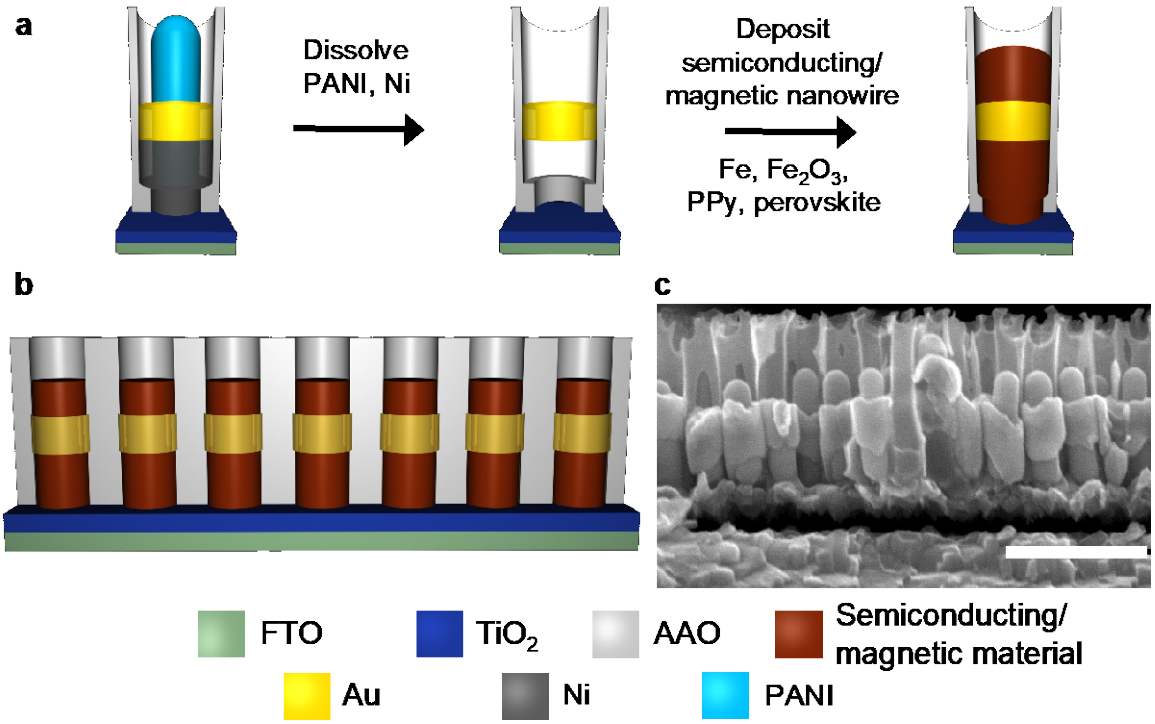

Figure 14. COAL within thin AAO templates bound to transparent conductive FTO/TiO_2 substrates. (a) Generalization of the nanowire core material *via* the COAL process. (b) Scheme of nanowire-nanoring array bound to a bulk conducting electrode. (c) Cross-sectional SEM image of Ni-Au shell segments around a polyaniline (PANI) core within thin AAO templates.

2. Plasmon-exciton interactions in DNA-nanoparticle superlattices (Mirkin group)

The incorporation of dye molecules into the single crystalline nanoparticle superlattices allows the study of interactions among photonic, plasmonic, and excitonic modes. On one hand at the nanoscale, the interaction between the dye dipoles and surface plasmons can be finely tuned by positioning the dye molecules to specific sites of the DNA particle-linker strands, thereby modulating dye-nanoparticle distance, as briefly mentioned in the previous section. On the other hand, the microscopic anisotropic geometry of the superlattices, as represented as the rhombic dodecahedral crystal habit, couples with photonic modes to give directional light emission. DNA-mediated colloidal crystallization offers individual control of these two aspects, and interesting coupling behavior was probed by an experiment performed by the Mirkin group (**Figure 15)**. By using a laser with a wavelength that matches the absorption peak of the dye, in this case 504 nm, dye molecules in the superlattices are excited, and they fluoresce at 550 nm. However, light emitted or transmitted through the center of the superlattice is absorbed by Au nanoparticles, and thus, only the light emitted at the vertices of the rhombic dodecahedral crystal can be observed when the focal plane of the objective lens is at the center of the superlattice (**Figure 15a**, top). Due to the interaction with Au nanoparticles, the dye molecules also fluoresce at longer wavelength (~650 nm). Since the extinction of Au nanoparticles is less significant at λ=650 nm, light at this wavelength passes through the superlattice and can be detected 3 μm below the superlattice (**Figure 15a**, bottom). Without the absorption of Au nanoparticles, the superlattice acts as an uncoupled ensemble of dye molecules, as can be seen in the control sample where the Au nanoparticles were etched away (**Figure 15c,d**). These initial proof-of-concept structures unambiguously show that one can obtain plasmonically modulated directional light emission. The DNA-guided approach to superlattice microcavities described herein provides a versatile platform for building photonic architectures with exciton emission behavior that can be modulated in the spatial, spectral, and time domains for various nano-/microphotonic

applications. In addition, the use of magnetic nanoparticles, for example, magnetite (Fe_3O_4), as the core materials for this type of colloidal crystallization, enables researchers to investigate the spin- and surface ligand-guided interactions between the magnetic nanoparticles themselves, or more interestingly, magnetoplasmonic interactions when co-crystallized with plasmonic nanoparticles.

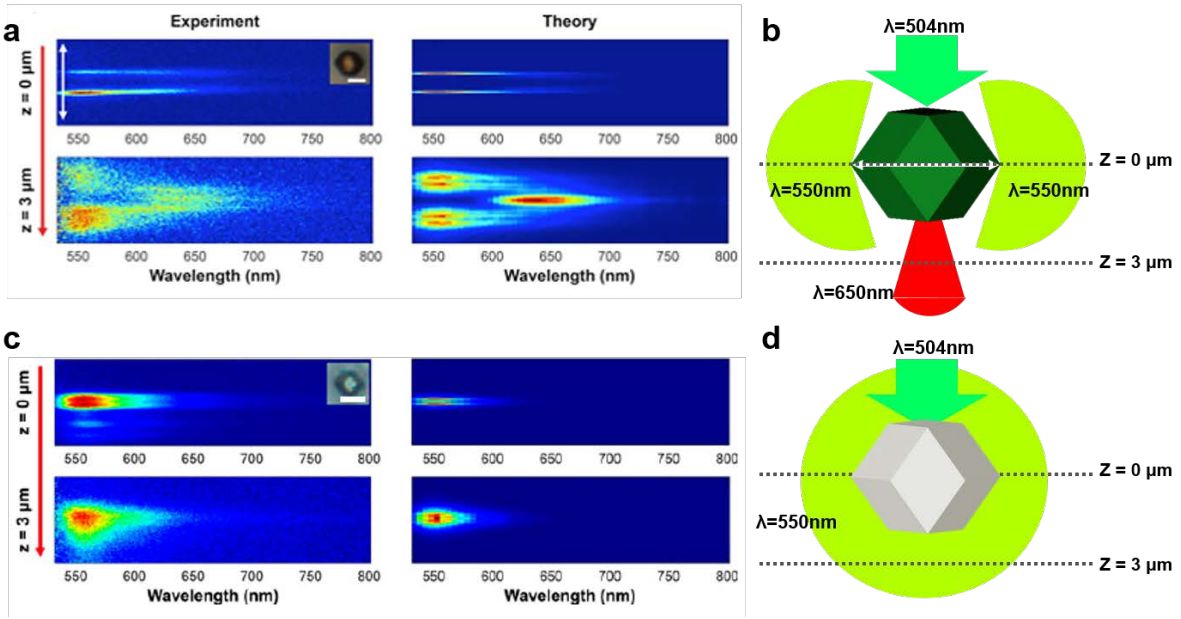

Figure 15. Spatio-spectral analysis of microcavity dye emission. Laser pulses (λ = 504 nm, pulse width ~100 ps, spot size of ~5 –10 μm) were used in transmission mode and focused through a 100× objective lens to excite a single superlattice. (a) Spatio-spectral emission profile (Left) of a superlattice (L ~5 μm, Inset) compared with the theoretical prediction (Middle). The top images were formed with the focal plane located around the center of the superlattice, and the bottom images with the focal plane 3 μm below it (see the scheme in the (b)). Emitted light was collected with a slit cutting through the center of the superlattice (white arrow in (b)) where spatial (vertical axis of the profile, 30 μm) and spectral information (horizontal axis of the profile) were collected simultaneously. (c) Comparable data for a Au-etched control superlattice were investigated to analyze the effect of plasmonic absorbers. The Au-etched control superlattice is transparent under optical microscope due to lack of nanoparticle scattering (Inset). These results of emission behaviors of superlattices in (a) and (c) are described in schemes in (b) and (d), respectively. (Scale bar, 5 μm.)

3. Direct observation of PICS in metal NP/semiconductor NW hybrid system (Jang group)

To evaluate role of the AgNP at a junction between a AgNP and a p-type PPy NW, KPFM measurement on AgNP-attached PPy NWs (PPy_{AgNP} NW) were carried out (**Figure 16**). A surface potential (V_{CPD}) image in dark mode (normal KPFM) of the PPy_{AgNP} NW is displayed with a simultaneously observed topographic image. A line-profile of surface potential at the interface between the AgNP and PPy NW of the PPy_{AgNP} NW is displayed with that of the PPy NW and Ag NP. The blue arrow indicates that the surface potential of PPy NW decreases at the interface, while that of the AgNP increases (indicated by the red arrow). This means that negative charges (electrons) increase at the interface of the PPy NW, and negative charges (electrons) decrease at the interface of the AgNP.

DISTRIBUTION A. Approved for public release: distribution unlimited.

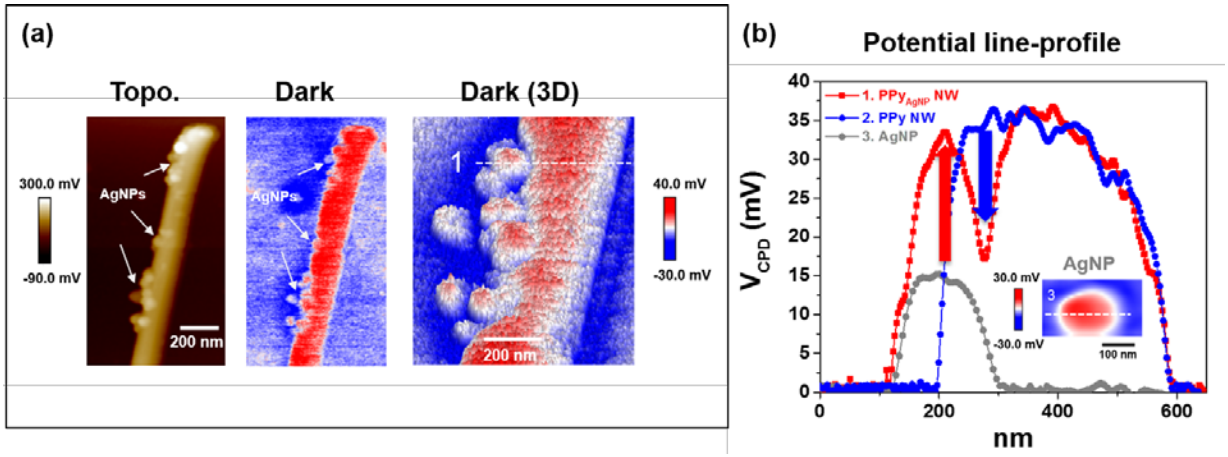

Figure 16. (a) Topographic image and KPFM images of PPy$_{AgNP}$ NW. (b) Surface potential line-profiles of PPy$_{AgNP}$ NW, PPy NW, and AgNP. Changes of surface potential at junction and non-junction of AgNP and PPy NW are displayed as red and blue arrows, respectively.

The surface potential of PPy$_{AgNP}$ NW in plasmonic excitation was measured by KPFM with blue light (λ=450 nm) irradiation. Because the plasmonic absorption peak of the AgNPs and absorption peak of the PPy NWs exist between 400 nm – 500 nm, plasmonic excitation of the AgNP as well as excitonic excitation of the PPy NW will occur with blue light irradiation. Surface potential line-profiles of the AgNP, PPy NW, and PPy$_{AgNP}$ NW are displayed in **Figure 17b**. The blue arrow indicates that the surface potential of PPy NW increases at the interface, while that of AgNP decreases (red arrow). On the contrary, in the dark for the PPy$_{AgNP}$ NW system, negative charges (electrons) decrease and increase at the interface of PPy and AgNP, respectively. This implies that the AgNP works as an "electron donor" in initial contact with PPy NW and works as an "electron accepter" in the plasmonic excitation mode.

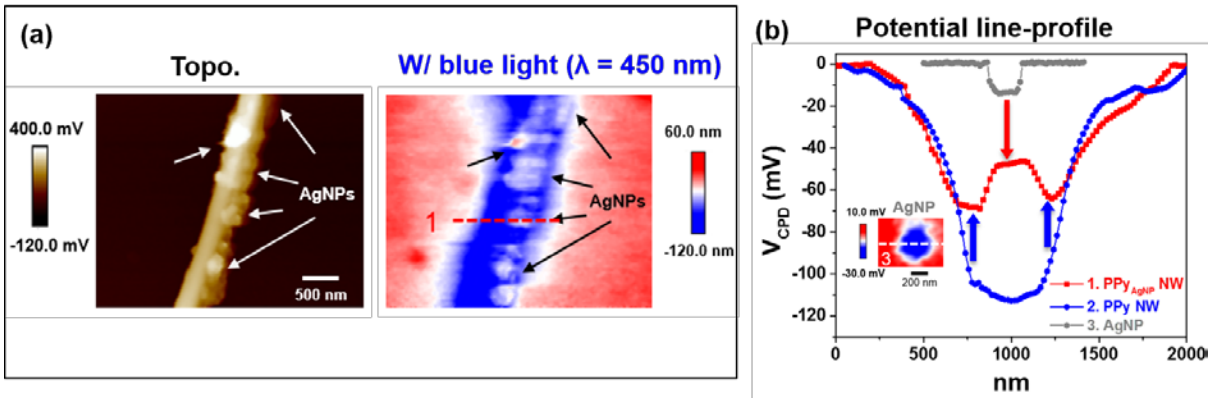

Figure 17. (a) Topographic image and blue light irradiated KPFM image of PPy$_{AgNP}$ NW. (b) Surface potential line-profiles of PPy$_{AgNP}$ NW, PPy NW, and AgNP. Changes of surface potential at junction and non-junction of AgNP and PPy NW are displayed as red and blue arrows, respectively.

As a control experiment, light-irradiated KPFM measurements of AuNPs attached to n-type ZnO NWs (ZnO$_{AuNP}$ NW) were carried out. To lower the Fermi energy, an n-type ZnO NW was introduced, where upward bending of the energy band of the semiconductor NW is anticipated at the interface with AuNP. A KPFM image of a ZnO$_{AuNP}$ NW in the dark (normal KPFM) and the change of surface potentials of the ZnO NW and AuNP at the junction are displayed in **Figure 18b**. The blue arrow indicates that the surface potential of ZnO NW increases at the interface, which means the amount of negative charges (electrons)

DISTRIBUTION A. Approved for public release: distribution unlimited.

decreases. Whereas, the surface potential of the AuNP decreases at the interface (red arrow), which means that negative charges (electrons) increase at the interface of the AuNP.

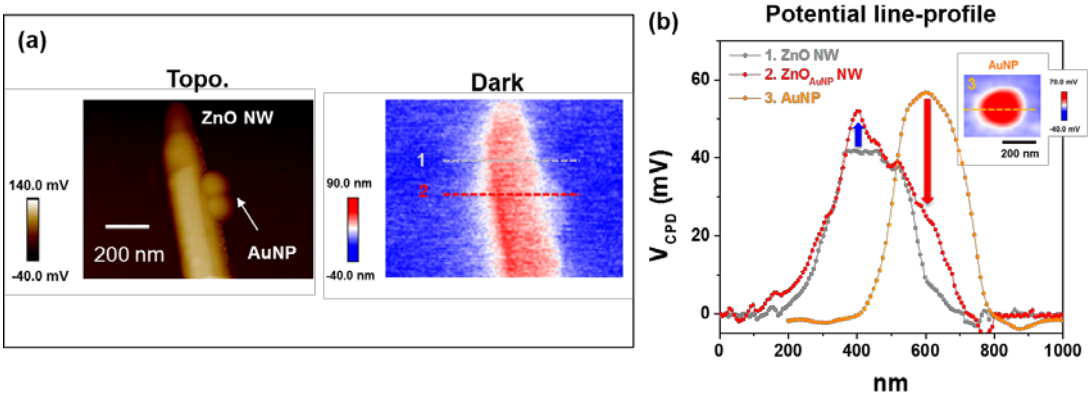

Figure 18. (a) Topographic image and KPFM image of ZnO_{AuNP} NW. (b) Surface potential line-profiles of ZnO NW, ZnO_{AuNP} NW, and AuNP. Changes of surface potential at junction and non-junction of ZnO NW and AuNP are displayed as red and blue arrows, respectively.

The surface potential of the ZnO_{AuNP} NW in plasmonic excitation by green light (λ = 550 nm) irradiation was measured (**Figure 19a**). The plasmonic absorption peak of the AuNPs exists around 550 nm. **Figure 19b** shows that the surface potentials of ZnO NW and AuNP oppositely change in plasmonic excitation mode. The blue arrow indicates the decreasing surface potential of ZnO region, while the red arrow indicates the increasing surface potential of the AuNP region in the ZnO_{AuNP} NW by green light irradiation. This result means that negative charges (electrons) decrease and increase, respectively, in the ZnO region and the AuNP region in plasmonic excitation mode of ZnO_{AuNP} NW.

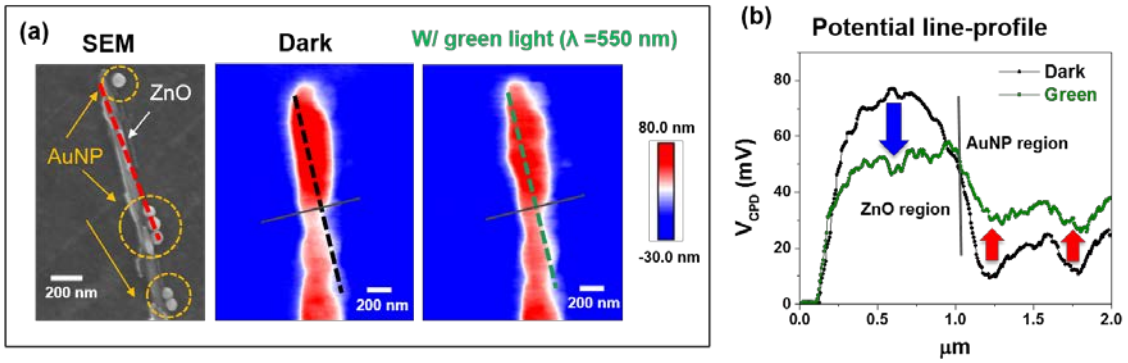

Figure 19. (a) Topographic image and green light irradiated KPFM image of ZnO_{AuNP} NW. (b) Surface potential line-profiles of ZnO_{AuNP} NW in dark mode and in plasmonic excitation mode (green light irradiation). Changes of surface potential in the ZnO and AuNP region by plasmonic excitation are displayed as blue and red arrows, respectively.

In **Figure 20**, the changes of surface potential of the PPy_{AgNP} NW and the ZnO_{AuNP} NW in the dark and plasmonic excitation modes are summarized as bar graphs. For the PPy_{AgNP} NW system, the AgNP initially (dark mode) works as “electron donor” and then works as an “electron accepter” in plasmonic excitation mode by blue light irradiation. However, the AuNP in the ZnO_{AuNP} NW works as an “electron accepter” in the initial dark mode and works as an “electron donor” in the plasmonic excitation mode (green light irradiation). Hence, we can conclude that metal NPs behavior as either electron donors or acceptors depending on the type of semiconductor NW used.

DISTRIBUTION A. Approved for public release: distribution unlimited.

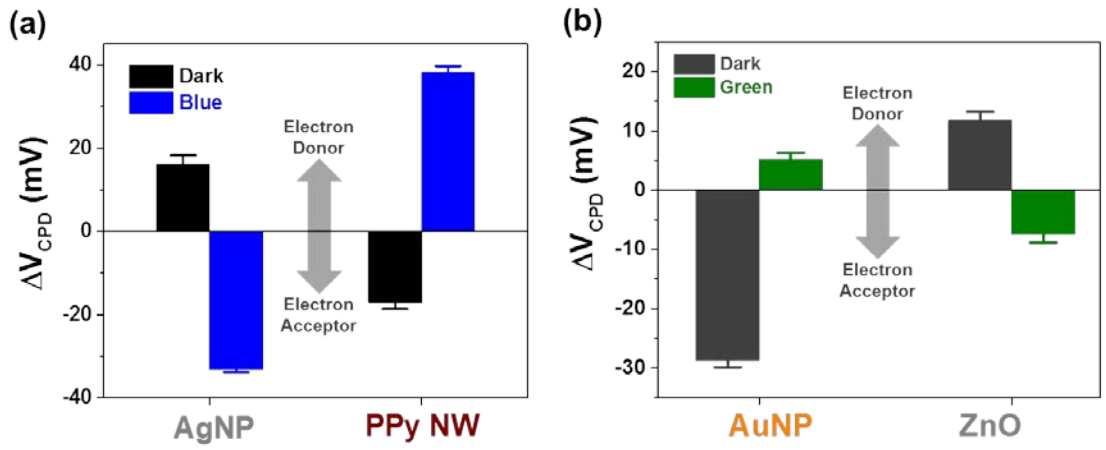

Figure 20. Difference of surface potentials of (a) PPy_{AgNP} NW and (b) ZnO_{AuNP} NW in dark and plasmonic excitation modes. Opposite behaviors of metal NP and semiconductor NW in PPy_{AgNP} NW and ZnO_{AuNP} NW are observed.

The Jang group has characterized the role of the metal NP in the metal/semiconductor nanostructured junction with plasmonic excitation of the metal NP. The type of the semiconductor NW is important to determine whether the metal NP works as a electron donor or acceptor. This discovery demonstrates a way to control electron movement in metal/semiconductor nanostructured junctions by means of matching the energy bandgaps of the metal and semiconductor.

4. Spin-coupled plasmonic interactions (Jang group)

In the case of the characterization of the spin-coupled plasmonic interactions of the Fe NW with Au double rings, the surface potential difference of the NW depending on the alignment of the magnetic moment in the NW has been characterized by light-irradiated KPFM measurement. In **Figure 21**, schemes of two different alignments of the NW are displayed with MFM images; the +z direction represents the magnetic moment alignment perpendicular to the NW axis ($\mu \parallel +z$), while the +y direction represents magnetic moment alignment parallel to the NW axis ($\mu \parallel +y$). Line profiles of surface potential along with the NWs in three different conditions (dark, LSPR on and off) are summarized in **Figure 21b-c**. When the magnetic moment alignment is perpendicular to the NW axis ($\mu \parallel +z$), the difference between the surface potentials in dark and light irradiation (ΔV_{CPD}) are relatively larger than the ΔV_{CPD} when the magnetic moment alignment is perpendicular to the NW axis ($\mu \parallel +y$) (**Figure 21d-f**). In the result, we noticed that the surface potential difference reveals three insights: ΔV_{CPD} at the Au double rings is smaller than that at the Fe NW region, ΔV_{CPD} under LSPR is larger than that in the LSPR off condition, and ΔV_{CPD} when the H-field compartment of the irradiating light is perpendicular to the magnetic moment of the NW ($\mu \parallel +y$) is smaller than that when thebH-field compartment of the irradiating light is parallel to it ($\mu \parallel +z$). From these observations, spin-coupled plasmonic interactions can be characterized, providing a way to manipulate plasmonic excitations by controlling the spin alignment of the sample system.

DISTRIBUTION A. Approved for public release: distribution unlimited.

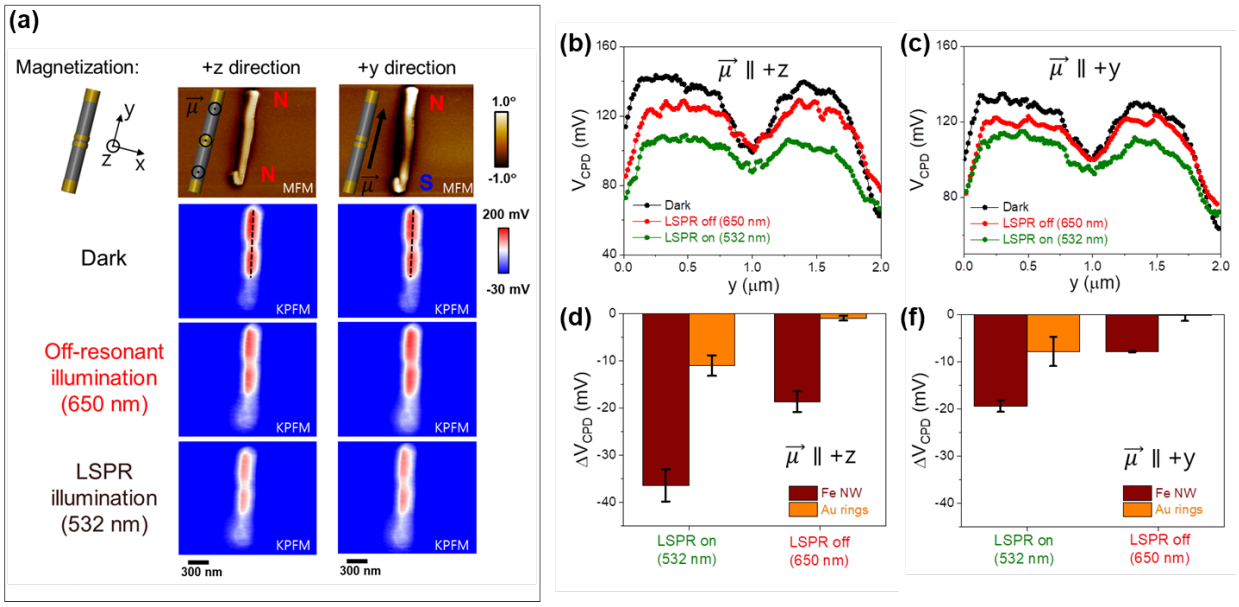

Figure 21. (a) Scheme of aligning magnetic moment and surface potential mappings of Fe NW with Au double rings. (b, c) line profiles and (d,f) bar graphs of surface potential and its difference depending on magnetic moment alignment.

List of Publications and Significant Collaborations that resulted from your AOARD supported project: In standard format showing authors, title, journal, issue, pages, and date, for each category list the following:

a) papers published in peer-reviewed journals,

The Mirkin Group

1. Zhou, X.; Zhou, Y.; Ku, J.; Zhang, C.; Mirkin, C. A. "Capillary Force-driven, Large-area Alignment of Multi-Segmented Nanowires," *ACS Nano*, **2014**, *8*, 1511-1516.
2. Zhou, Y.; Zhou, X.; Park, D.; Torabi, K.; Brown, K.; Jones, M. R.; Zhang, C.; Schatz, G. C.; Mirkin, C. A. "Shape-Selective Deposition and Assembly of Anisotropic Nanoparticles," *Nano Lett.*, **2014**, *14*, 2157-2161.
3. Mangelson, B. F.; Jones, M. R.; Park, D. J.; Shade, C. M.; Schatz, G. C.; Mirkin, C. A. "Synthesis and Characterization of a Plasmonic-Semiconductor Composite Containing Rationally Designed, Optically Tunable Gold Nanorod Dimers and Anatase TiO2," *Chem. Mater.*, **2014**, *26*, 3818-3824.
4. Osberg, K. D.; Harris, N.; Ozel, T.; Ku, J. C.; Schatz, G. C.; Mirkin, C. A. "A Systematic Study of Antibonding Modes in Gold Nanorod Dimers and Trimers," *Nano Lett.*, **2014**, *14*, 6949-6954.
5. Ozel, T.; Bourret, G. R.; Mirkin, C. A. "Coaxial Lithography," *Nat. Nanotechnol.*, **2015**, *10*, 319-324.
6. Ozel, T.; Ashley, M. J.; Bourret, G. R.; Ross, M. B.; Schatz, G. C.; Mirkin, C. A. "Solution-Dispersible Metal Nanorings with Deliberately Controllable Compositions and Architectural Parameters for Tunable Plasmonic Response," *Nano Lett.*, **2015**, *15*, 5273-5278.
7. Liu, Z.; Sun, J.; Zhou, Y.; Zhang, Y.; Wu, Y.; Nalluri, S. K. M.; Wang, Y.; Samanta, V.; Mirkin, C. A.; Schatz, G. C.; Stoddart, J. F. "Supramolecular Gelation of Rigid Triangular Macrocycles Through Rings of Multiple C-O•••O Interactions Acting Cooperatively," *J. Org. Chem.*, **2016**, *81*, 2581-2588.
8. Chen, P. C.; Liu, X.; Hedrick, J. L.; Xie, Z.; Wang, S.; Lin, Q. Y.; Hersam, M. C.;

Dravid, V. P.; Mirkin, C. A. “Polyelemental nanoparticle libraries,” *Science*, **2016**, *352*, 1565-1569.
9. Ashley, M. J.; O’Brien, M. N.; Hedderick, K. R.; Mason, J. A.; Ross, M. B.; Mirkin, C. A. “Templated Synthesis of Uniform Pervskite Nanowire Arrays,” *J. Am. Chem. Soc.*, **2016**, *138*, 10096-10099.
10. Hou, X.; Ke, C.; Zhou, Y.; Xie, Z.; Alngadh, A.; Keane, D. T.; Nassar, M. S.; Botros, Y. Y.; Mirkin, C. A.; Stoddart, J. F. “Concurrent Covalent and Supramolecular Polymerization,” *Chem. Eur. J.*, **2016**, *22*, 12301-12306.
11. Park, D. J.*; Ku, J. C.*; Sun, L.; Lethiec, C. M.; Stern, N. P.; Schatz, G. C.; Mirkin C. A. “Directional Emission from Dye-Functionalized Plasmonic DNA Superlattice Microcavities,” *Proc. Natl. Aced. Sci. U. S. A.*, **2017**, *114*, 457-461.
12. Sun, L.; Lin, H.; Park, D. J.; Bourgeois M. R.; Ross, M. B.; Ku, J. C.; Schatz, G. C.; Mirkin, C. A. “Polarization-Dependent Optical Response in Anisotropic Nanoparticle–DNA Superlattices,” *Nano Lett.*, **2017**, *17*, 2313-2318.
13. Oh, T.; Ku, J. C.; Ozel, T.; Mirkin, C. A. “Orthogonal Chemical Modification of Template-Synthesized Nanostructures with DNA,” *J. Am. Chem. Soc.*, **2017**, *139*, 6831-6834.
14. Xie, Z.; Gordiichuk, P.; Lin, Q.-Y.; Meckes, B.; Chen, P.-C.; Sun, L.; Du, J. S.; Zhu, J.; Liu, Y.; Dravid, V. P.; Mirkin, C. A. “Solution-Phase Photochemical Nanopatterning Enabled by High-Refractive-Index Beam Pen Arrays,” *ACS Nano*, **2017**, *11*, 8231-8241.

The Jang Group
15. Yang, M.-S.; Son, S.-J.; Park; B.; Moon, B. K.; Jang, J.-W. “Fabrication and optical properties of zirconia nanoparticle array on a patterned hydrophilic-hydrophobic substrate,” *J. Appl. Phys.*, **2013**, *114*, 23406.
16. Park, B.; Noh, H.; Yu, Y. M.; Jang, J.-W. “Finite-difference time-domain analysis on light extraction in a GaN light-emitting diode by empirically capable dielectric nano-features,” *J. Appl. Phys.*, **2014**, *116(18)*, 184302.
17. Jang, J.-W.; Park, B.; Nettikadan, S.; “Generation of Plasmonic Au Nanostructures in the Visible Wavelength Using Two-Dimensional Parallel Dip-Pen Nanolithography,” *Nanoscale*, **2014**, *6*, 7912-7916.
18. Lee, S.-H.; Yang, M.-S.; Jang, J.-W.; Min, C.; Kim, Y. “A Micro-fabrication Tool for Automatic Large-area Patterning Using Polymer Pen Lithography,” *New Phys.: Sae Mulli*, **2015**, *65(6)*, 615-620.
19. Lee, S.-H.; Bae, J.; Lee, S.W.; Jang, J.-W. “Improvement of Polypyrrole Nanowire Devices by Plasmonic Space Charge Generation: High Photocurrent and Wide Spectral Response by Ag Nanoparticle Decoration,” *Nanoscale*, **2015**, *7*, 17328-17337.
20. Lee, S.-H.; Shin, M.; Hwang, S.; Jang, J.-W. “Unconventional but tunable phase transition above the percolation threshold by two-layer conduction in electroless-deposited Au nanofeatures on silicon substrate,” *Nanotechnology*, **2015**, *26*, 505202.
21. Yang, M.-S.; Lee, S.-H.; Moon, B. K.; Yoo, S. R.; Hwang, S.; Jang, J.-W. “Critical Role of Wettability in Assembly of Zirconia Nanoparticles on a Self-assembled Monolayer-Patterned Substrate,” *J. Appl. Phys.*, **2016**, *120*, 085304.
22. Lee, S.-H.; Hwang, S.; Jang, J.-W. “Giant Temperature Coefficient of Resistivity and Cryogenic Sensitivity in Silicon with Galvanically Displaced Gold Nanoparticles in Freeze-Out Region,” *ACS Nano*, **2017**, *11*, 1572−1580.
23. Oh, C.-M.; Park, K. H.; Choi, J.-H.; Hwang, S.; Noh, H.; Yu, Y. M.; Jang, J.-W. “Polycrystalline Au Nanomembrane as a Tool for Two-Tone Micro/Nanolithography,” *Chemistry of Materials*, **2017**, *29*, 3863–3872.

DISTRIBUTION A. Approved for public release: distribution unlimited.

Mirkin-Jang Collaboration

24. Lim, J. K.; Lee, O. –S.; Jang, J. –W.; Petrosko, S. H.; Schatz, G. C.; Mirkin, C. A. "Molecular Transport Junctions Created by Self-Contacting Gapped Nanowires," *Small*, **2016**, *12*, 4349-4356.

b) papers published in peer-reviewed conference proceedings,
Nothing to report.

c) papers published in non-peer-reviewed journals and conference proceedings,
Nothing to report.

d) conference presentations without papers,
Chad A. Mirkin

1. ACS National Meeting, Indianapolis, IN; "Ternary Nanoparticle Superlattices through Topoactic Intercalation" (2013).
2. AbbVie Biotech Ventures Inaugural CEO Forum, Lake Forest, IL; "Exploiting Proprietary Spherical Nucleic Acid (SNA) Platform to Target Disease Genetically" (2013).
3. NCI Alliance in Cancer Meeting, Bethesda, MD; "Spherical Nucleic Acids (SNAs) for the Treatment of Glioblastoma" (2013).
4. Chevron Phillips Chemical Co. LP, Bartlesville, OK; "Nanotechnology: Learning to Think Big in a Field Focused on the Small" (2013).
5. University of Portland, Linus Pauling Medal Symposium, Portland, OR; "Programmable Atom Equivalents from Spherical Nucleic Acid (SNA) Nanoparticle Conjugates: Defining a New 'Table of Elements'" (2013).
6. University of Portland, Linus Pauling Medal Symposium, Portland, OR; "Nanotechnology: Moving Beyond Small Thinking" (2013).
7. Corning, Inc., Painted Post, NY; "A Chemist's Approach to Nanofabrication: Towards a 'Desktop Fab'" (2013).
8. Princeton University, Crocco Colloquium, Princeton, NJ; "Nucleic Acid-Modified Nanostructures as Programmable Atom Equivalents: Forging a New 'Table of Elements'"(2013).
9. Princeton University, Crocco Colloquium, Princeton, NJ; "A Chemist's Approach to Nanofabrication: Towards a 'Desktop Fab'"(2013).
10. Fudan University, Interfacing of Materials and Biology Symposium, Shanghai, China; "Spherical Nucleic Acid Nanoparticle Conjugates: A New Approach to Intracellular Gene Regulation" (2013).
11. Nanyang Technological University, Singapore; "Novel Methods of Biodetection Upon Structurally Well-Defined Nano Particle Probes" (2013).
12. The Scientific Research Society (Sigma Xi), Student Research Conference, Raleigh, NC; (2013).
13. Southeast Regional ACS Meeting, Symposium of Nanochemistry and Spectroscopy, Atlanta, GA; "A Chemist's Approach to Nanofabrication: Towards a 'Desktop Fab'" (2013).
14. DARPA/ MTO PI Review meeting for the In Vivo Nanoplatforms (IVN) Program, Arlington, VA; "Spherical Nucleic Acids for In Vivo Therapeutics" (2013).
15. De Long Annual Natural Materials and Systems Program Review, Fort Walton Beach, FL; "MURI: BioProgrammable One-, Two-, and Three-Dimensional Materials" (2013).

16. De Long Annual Natural Materials and Systems Program Review, Fort Walton Beach, FL; "Nanostructured Interfaces and Patterning Tools for Probing Bioinspired Materials and Systems" (2013).
17. 12th US-Japan Symposium on Drug Delivery Systems, Lahaina, Maui, Hawaii; "Spherical Nucleic Acid (SNA) Nanostructures: Establishing a New Paradigm in Molecular Diagnostics and Intracellular Gene Regulation" (2013).
18. Workshop on Advanced Materials, Ras al Khaimah, Qatar; "Spherical Nucleic Acid (SNA) Nanostructures: Establishing a New Paradigm in Molecular Diagnostics and Intracellular Gene Regulation" (2014).
19. International Workshop on Advanced Materials, Dubai, UAE; "Spherical Nucleic Acids as Programmable Atom Equivalents: Constructing a New 'Table of Elements'" (2014).
20. PITTCON, Chicago, IL; "Spherical Nucleic Acids (SNAs): Novel Therapeutic Agents for Cancer Treatment" (2014).
21. PITTCON, Chicago, IL; "A Chemist's Approach to Nanofabrication: Towards a 'Desktop Fab'" (2014).
22. American Chemical Society, Dallas, TX; "Nucleic Acid-Modified Nanostructures as Programmable Atom Equivalents: Forging a New 'Table of Elements'" (2014.)
23. American Chemical Society, Dallas, TX; "'Nano-flares' for the Analysis of Circulating Cancer Cells" (2014).
24. American Chemical Society, Dallas, TX; "Spherical Nucleic Acid (SNA) Nanostructures: Establishing a New Paradigm in Molecular Diagnostics and Intracellular Gene Regulations" (2014).
25. American Association for the Advancement of Science, Chicago, IL; "Convergence Science: A Revolution for Health Solutions" (2014).
26. American Association for Cancer Research, San Diego, CA; "Spherical Nucleic Acids for the Treatment of Glioblastoma Multiforme" (2014).
27. In Vivo Nanoplatforms Review, San Diego, CA; "Spherical Nucleic Acids for In Vivo Therapeutics" (2014).
28. California Institute of Technology, Pasadena, CA; "Spherical Nucleic Acid (SNA) Nanostructures: Establishing a New Paradigm in Molecular Diagnostics and Intracellular Gene Regulation" (2014).
29. Nanjing University of Technology, Nanjing, China; "Spherical Nucleic Acids: A New Paradigm in Intracellular Gene Regulation and Molecular Diagnostics" (2014).
30. Nanjing University of Technology, Nanjing, China; "Cantilever-free Molecular Printing: Toward a 'Desktop Fab'" (2014).
31. The Sixth International Symposium on Bioanalysis, Biomedical Engineering, and Nanotechnology, Hunan University, Changsha, China; "Intracellular Fate of Spherical Nucleic Acid Nanoparticle Conjugates" (2014).
32. The Tenth Nanoscience and Nanotechnology Conference, Istanbul, Turkey; "Nucleic Acid-Modified Nanostructures as Programmable Atom Equivalents: Forging a New 'Table of Elements'" (2014).
33. Gordon Research Conferences Bioanalytical Sensors, Salve Regina University, Providence, Rhode Island; "'Nano-flares' for the Analysis of Circulating Cancer Cells" (2014).
34. The Twelfth International Conference on Nanostructured Materials, Moscow, Russia; "Spherical Nucleic Acid (SNA) Nanostructures as Intracellular Probes and Gene Regulation Agents" (2014).
35. NBIT Program Review and Nanoscience Technical Exchange, University of California, Berkeley, CA; "Plasmonic Optoelectronic Interactions" (2014).

DISTRIBUTION A. Approved for public release: distribution unlimited.

36. 2014 Annual Beckman Symposium, Irvine, CA; “The Nature of the DNA Bond” (2014).
37. 248th ACS National Meeting, San Francisco, CA; “Materials by design from programmable atom equivalents (PAEs)” (2014).
38. 248th ACS National Meeting, San Francisco, CA; “Coaxial lithography” (2014).
39. 248th ACS National Meeting, San Francisco, CA; “Spherical nucleic acid (SNA) nanostructures: Enabling tools for biomedical applications” (2014).
40. 248th ACS National Meeting, San Francisco, CA; “Nature and implications of near-perfect nanoparticle seeds” (2014).
41. ISACS Meeting on Nanoscience, San Diego, CA; “Spherical Nucleic Acids as Programmable Atom Equivalents: Constructing a New ‘Table of Elements’” (2014).
42. Fermilab Arts & Lecture Series, Batavia, IL; “Nanotechnology: Learning to think big in a field focused on the small” (2014).
43. NCI Alliance for Nanotechnology in Cancer Annual Investigator’s Meeting, Rockville, MD; “Nanomaterials for Cancer Diagnostics and Therapeutics” (2014).
44. SmithGroupJJR Distinguished Lecture, Beckman Institute for Advanced Science and Technology, UIUC, Urbana, IL; “The Nature of the DNA Bond” (2014).
45. Multidisciplinary Chemistry Without Borders, Porto Alegre, Brazil; “Cantilever-Free Scanning Probe Lithography: Towards a ‘Desktop Fab’” (2014).
46. Multidisciplinary Chemistry Without Borders, Porto Alegre, Brazil; “Revolutionizing the field of medicine through advances in nanotechnology” (2014).
47. American Association of Pharmaceutical Scientists Annual Meeting and Exposition, San Diego, CA; “Spherical Nucleic Acid (SNA) Nanostructures for Advanced Wound Healing Applications” (2014).
48. UCSD Department of Bioengineering, Skalak Memorial Lecture, San Diego, CA; “Spherical Nucleic Acid (SNA) Nanostructures as Intracellular Probes and Gene Regulation Agents” (2014).
49. Army Research Laboratory Colloquium Series, Aberdeen Proving Ground, MD; “Spherical Nucleic Acids as Programmable Atom Equivalents: Constructing a New "Table of Elements"” (2014).
50. American Society of Nephrology, Kidney Week 2014, Philadelphia, PA; “Realizing the Promise of Nanomedicine” (2014).
51. Korean Academy of Science and Technology, Distinguished Lecture, Seoul National University, Seoul, South Korea; “Programmable Atom Equivalents from Nucleic-Acid Modified Nanostructures: Constructing a New ‘Table of Elements’” (2014).
52. Korea Academy of Science and Technology, Prestige Workshop, Seoul National University, Seoul, South Korea; “Biological Properties of Spherical Nucleic Acids” (2014).
53. Korean Academy of Science and Technology, Pioneers in Photonic Nanostructures and Nanophotonics Symposium, Seoul National University, Seoul, South Korea; “Plasmonic Nanostructures and Assemblies Based Upon Them” (2014).
54. EMBS Micro and Nanotechnology in Medicine Conference, Oahu, Hawaii; “Spherical Nucleic Acid (SNA) Nanostructures as Intracellular Probes and Gene Regulation Agents” (2014).
55. PITTCON, New Orleans, LA; “Liposomal SNAs: A New Approach to Gene Regulation Therapy” (2015)
56. ACS Spring 2015 National Meeting, Denver, CO; “Nanotechnology: Delivering the Promise - R&D” (2015).

57. ACS Spring 2015 National Meeting, Denver, CO; “Programmable Atom Equivalents from Nucleic-Acid Modified Nanostructures: Constructing a New ‘Table of Elements’” (2015).
58. MRS 2015 Spring Conference, San Francisco, CA; “Liposomal Spherical Nucleic Acids: A New Approach to Immuno-Modulatory and Regulation Therapies” (2015).
59. MRS 2015 Spring Conference, San Francisco, CA; “The Nature and Implications of Near-Perfect Nanoparticle Seeds” (2015).
60. MRS 2015 Spring Conference, San Francisco, CA; “The Design Principals for Colloidal Crystals made from Proteins Modified with Nucleic Acids” (2015).
61. Workshop in NanoScience and NanoEngineering, Duke University, Durham, NC; “Programmable Atom Equivalents from Nucleic-Acid Modified Nanostructures: Forging a New ‘Table of Elements’” (2015).
62. National Security Science and Engineering Faculty Fellowship 2014 Class Orientation, Arlington, VA; “Functional Crystals through Encodable Hard and Soft Matter” (2015).
63. Phi Lambda Upsilon-Rho Chapter Award Lecture, University of Nebraska – Lincoln, Lincoln, NE: “The Nature of the DNA Bond” (2015).
64. Department of Chemistry Inorganic Harvard/MIT Seminar Series, MIT, Cambridge, MA; “Spherical Nucleic Acids as Programmable Atom Equivalents: Constructing a New ‘Table of Elements’” (2015).
65. UNC Center for Nanotechnology in Drug Delivery Eshelman School of Pharmacy Distinguished Speaker Seminar, Chapel Hill, NC; “Liposomal Spherical Nucleic Acids: A New Approach to Immunomodulatory Therapies” (2015).
66. CIC biomaGUNE Seminar, San Sebastian, Spain; “Programmable Atom Equivalents from Nucleic Acid-Modified Nanoparticle Constructs” (2015).
67. ICBN Workshop: Revolutionizing Biology and Medicine with Advances in Nanotechnology, Hunan University, Changsha, China; “Liposomal Spherical Nucleic Acids (SNAs): New and Potent Agents for Immunomodulatory Therapies” (2015).
68. ShanghaiTech Advances in Research (STAR) Symposium, Shanghai, China; “Liposomal Spherical Nucleic Acids: A New Approach to Immunomodulatory Therapies” (2015).
69. GRC Nucleosides, Nucleotides & Oligonucleotides, Salve Regina University, Newport, RI; “Programmable Materials and the Nature of the DNA Bond” (2015).
70. IARPA Bio Intelligence Chips Program PI Meeting, Livermore, CA; “Biodiagnostic Approaches to Human Profiling Through Nanomaterial Indicators” (2015).
71. Karle Symposium, University of Michigan, Ann Arbor, MI; ““Programmable Materials and the Nature of the DNA Bond” (2015).
72. ACS Fall National Meeting, Boston, MA; “Nature of the DNA Bond” (2015).
73. ACS Fall National Meeting, Boston, MA; “Spherical Nucleic Acids: A New Paradigm in Nucleic Acid Therapies” (2015).
74. Workshop on Enabling Future Health Care: the Role of Micro and Nano Technologies, Napa, CA; “Nanotechnology: Promise for Future Healthcare” (2015).
75. Frontiers Seminar, Case Western University, Cleveland, OH; “Programmable Materials and The Nature of the DNA Bond” (2015).
76. President’s Science Symposium, Bowdoin College, Brunswick, ME; “Nanotechnology: A Small World with Big Potential” (2015).
77. Department of NanoEngineering Seminar Series, UCSD, San Diego, CA; “Liposomal Spherical Nucleic Acids: A New Approach to Immunomodulatory Therapies (2015).
78. Illumina Scientific Advisory Board Meeting, San Diego, CA; “The Convergence of Nanoscience with Biology and Medicine” (2015).

79. Peking University, Beijing, China; "Nanocombinatorics Through Scanning-Probed Based Chemistry and Biology" (2015).
80. MRS Fall Meeting, Boston, MA, "Programmable Materials and the Nature of the DNA Bond" (2015).
81. MRS Fall Meeting, Boston, MA, "Advanced RNA Analysis in Live Cells via Stickyflare Nanoconjugates" (2015).
82. MRS Fall Meeting, Boston, MA, "Liposomal SNAs as Immunomodulatory Agents for Cancer Vaccines" (2015).
83. AFOSR Natural Materials and Systems Program Review, Destin, FL, "MURI: Nanostructured Interfaces and Patterning Tools for Probing Bioinspired Materials and Systems" (2015).
84. 13th US-Japan Symposium on Drug Delivery Systems, Maui, HI, "Liposomal SNAs as Powerful Immunomodulatory Agents" (2015).
85. DOE Energy Frontier Research Centers Center for Bio-Inspired Energy Science Mid-Term Review, Gaithersburg, MD, "Pluripotent Nanoparticles: Reconfigurable Programmable Atom Equivalents" (2016).
86. Air Force Research Laboratory Human Performance Seminar, Dayton, OH, "Profiling State of Health with Biomarkers Identified Based Upon Ultrahigh Sensitivity, Highly Multiplexed Assays" (2016).
87. Pittcon Conference, Atlanta, GA, "Tracking the Amount and Location of RNA in Single Cells" (2016).
88. Pittcon Conference, Atlanta, GA, "Liposomal SNAs: A New Approach to Immunomodulatory Therapy" (2016).
89. ACS Spring 2016 Conference, San Diego, CA, "Pluripotent nanoparticles with programmable and responsive DNA bonds" (2016).
90. ACS Spring 2016 Conference, San Diego, CA, "Liposomal spherical nucleic acids: Nanostructures enabling the potential of therapeutic nucleic acids" (2016).
91. ACS Spring 2016 Conference, San Diego, CA, "Nanocombinatorix via scanning probe block copolymer lithography" (2016).
92. Baylor University Medical Center at Dallas Internal Medicine Grand Rounds, Dallas, TX, "Realizing the Promise of Nanomedicine" (2016).
93. Baylor University Medical Center at Dallas Internal Medicine, Dallas, TX, "Spherical Nucleic Acids: A New Platform in Immunotherapy" (2016).
94. NSSEFF Spring Meeting, Adelphi, MD, "Functional Crystals through Encodable Hard and Soft Matter" (2016).
95. Royal Society of Chemistry Centenary Prize Lecture Series, Glasgow University, Glasgow, Scotland, "Programmable Atom Equivalents and the Nature of the DNA Bond" (2016).
96. Royal Society of Chemistry Centenary Prize Lecture Series, University of Oxford, Oxford, England, "Programmable Atom Equivalents and the Nature of the DNA Bond" (2016).
97. Royal Society of Chemistry Centenary Prize Lecture Series, Imperial College of London, London, England, "Programmable Atom Equivalents and the Nature of the DNA Bond" (2016).
98. Young Investigator Network Lecture Series, Karlsruhe Institute of Technology, Karlsruhe, Germany, "The Convergence of Nanoscience and Nanomedicine: New Approaches for Studying, Tracking, and Treating Disease" (2016).
99. Aerospace Medical Association 87th Annual Scientific Meeting, Atlantic City, NJ, "Biomarker Detection Using Spherical Nucleic Acids" (2016).

100. Wuxi University, China, "Programmable Materials and the Nature of the DNA Bond" (2016).
101. Fudan Materials Beyond Symposium, Fudan University, China, “Colloidal Crystallization with DNA: Unlocking the Source Code for Materials by Design” (2016).
102. The 7th International Symposium on Bioanalysis, Biomedical Engineering and Nanotechnology, Hunan University, Changsha, China, “Nanostructures for Tracking RNA in Live Cells with Single Cell Resolution” (2016).
103. Young Giants of Nanoscience 2016, The Hong Kong Polytechnic University, Hong Kong, “Unlocking the Materials Genome Through Nanocombinatorix” (2016).
104. Center of Excellence for Advanced Bioprogrammable Nanomaterials Annual Reivew, AFRL, Dayton, OH, “Screening Nanotube Catalysts through Scanning Probe Block Copolymer Lithography” (2016).
105. Center of Excellence for Advanced Bioprogrammable Nanomaterials Annual Reivew, AFRL, Dayton, OH, “Rapid Quantificiaion of Salivary Cortisol through Nanoflares” (2016).
106. Noble Metal Nanoparticles, Gordon Research Conference, Mount Holyoke College, South Hadley, MA, “Biological Probes and Immunomodulatory Agents Based Upon Spherical Nucleic Acid Gold Nanoparticle Conjugates” (2016).
107. AACR Special Conference on Engineering and Physical Sciences in Oncology, Boston, MA, “Spherical nucleic acids as a powerful new platform for cancer immunotherapy” (2016).
108. Center for Bio-Inspired Energy Science External Advisory Board Meeting “Colloidal Nanomaterials: From Transmutable Programmable Atom Equivalents to Nano-to-Macro Scale Crystals” (2016).
109. ACS Fall 2016 Conference, Philadelphia, PA, “Chemical & Engineering News Talented 12” (2016).
110. ACS Fall 2016 Conference, Philadelphia, PA, “Elucidating the nanomaterial genome with scanning probe block co-polymer lithography” (2016).
111. ACS Fall 2016 Conference, Philadelphia, PA, “Unlocking the potential of spherical nucleic acids in biology and medicine” (2016).
112. ACS Fall 2016 Conference, Philadelphia, PA, “Nanostructures for tracking RNA within living cell” (2016).
113. Pfizer Tissue Targeting Symposium, Boston, MA, “SNAs: A New Standard in Drug Development and Immunotherapy” (2016).
114. University of Toronto Chemistry Lecture, Toronto, Canada, “Establishing a Genetic Code for Unnatural Materials” (2016).
115. Annual Investigator’s Meeting of the NCI Alliance for Nanotechnology in Cancer, Bethesda, MD, “SNA-based Nano-vaccines” (2016).
116. Nanjing Tech University Lecture, Nanjing, China, “Unlocking the Materials Genome Through Nanocombinatorix” (2016).
117. Physical Biology Lecture, Shanghai Institute of Applied Physics, Chinese Academy of Sciences, Shanghai, China, “Establishing a Genetic Code for Unnatural Materials” (2016).
118. AFOSR Natural Materials and Systems Program Review, Fort Walton Beach, FL, “4D Nanoprinter for Making and Manipulating Macroscopic Material” (2016).
119. AFOSR Natural Materials and Systems Program Review, Fort Walton Beach, FL, “Nanostructured Interfaces and Patterning Tools” 2016.
120. Frontiers of Biological Engineering Distinguished Seminar Series, UC Boulder, Boulder, CO, “Establishing a Genetic Code for Unnatural Materials” (2017).

121. Washington Molecular Imaging and Therapy Center Symposium, University of Washington, Seattle, WA, "Spherical Nucleic Acids (SNAs) as a Powerful New Platform for Nucleic Acid Therapeutics" (2017).
122. Pittcon Conference, Chicago, IL, "Spherical Nucleic Acids as Potent Immunomodulation Agents for Cancer Therapy" (2017).
123. Pittcon Conference, Chicago, IL, "Nano-Enabled In Vitro and In Vivo Diagnostic Tools for Tracking and Treating Disease" (2017).
124. Symposium on Photonics Science and Technology, Duke University Fitzpatrick Institute for Photonics, "Unlocking the Potential of Spherical Nucleic Acids in Biology and Medicine" (2017).
125. American Physical Society Annual National Convention, New Orleans, LA, "Programming the Assembly of Unnatural Materials with Nucleic Acids" (2017).
126. Brookhaven National Laboratory Distinguished Lecture, Upton, NY, "Unlocking the Materials Genome Through Combinatorial Nanoscience" (2017).
127. ACS Spring Conference, San Francisco, CA, "Programmable Materials from DNA Bonds and Nanoparticle Atoms" (2017).
128. ACS Spring Conference, San Francisco, CA, "Spherical Nucleic Acids: Making a Case for Next-Generation Nucleic Acid Therapeutics" (2017).
129. ACS Spring Conference, San Francisco, CA, "Modular Nanostructures for Immunotherapy" (2017).
130. ACS Spring Conference, San Francisco, CA, "Supramolecular Approach to Enzyme Mimics" (2017).
131. American Urological Association Annual Meeting, Boston, MA, "Spherical Nucleic Acids and their role in Digital Drug Design" (2017).
132. Nanomanufacturing: From Fundamentals to Scale-Up, Ann Arbor, MI, "Unlocking the Materials Genome through Nanocombinatorics" (2017).
133. Koch Institute's 16th Annual Research Symposium on the Convergence of Science and Engineering in Cancer Research, Cambridge, MA, "Spherical Nucleic Acids as a Powerful New Platform for Cancer Therapy" (2017).
134. Gordon Research Seminar, Cancer Nanotechnology, West Dover, VT, "Spherical Nucleic Acids as a Powerful New Platform to Develop Cancer Vaccines" (2017).
135. Gordon Research Conference, Cancer Nanotechnology, West Dover, VT, "Spherical Nucleic Acids for Cancer Immunotherapy and Gene Regulation" (2017).
136. Chemistry Beyond the Mechanical Bond, Cambridge, United Kingdom, "Crystal Engineering with DNA" (2017).
137. 3rd CIRP Conference on BioManufacturing, Chicago, IL, "Programming the Formation of Optically-Active Colloidal Crystals with DNA" (2017).
138. Centre for Supramolecular Chemistry Research, Cape Town, South Africa, "Ushering in the Digital Drug Design Revolution with Spherical Nucleic Acids" (2017).
139. ARO Chemical Sciences Division Program Review, Durham, NC, "Infinite Coordination Polymer Particles from Polymeric Coordinating Precursors" (2017).
140. ACS Fall Conference, Washington, DC, "Nanopatterned Extracellular Matrices Enable Cell-Based Assays with a Mass Spectrometric Readout" (2017).
141. ACS Fall Conference, Washington, DC, "Spherical Nucleic Acids as Potent Immunostimulatory Agents in Cancer" (2017).
142. ACS Fall Conference, Washington, DC, "Colloidal Crystal Engineering with DNA" (2017).
143. ACS Fall Conference, Washington, DC, "Unlocking the Materials Genome through Combinatoric Nanoscience" (2017).

144. Beihang University Advanced Innovation Center Lecture, Beijing China, “Combinatorial Nanoscience” (2017).
145. Sixth International Conference on DNA Nanotechnology, Beijing, China, “Crystal Engineering with DNA” (2017).
146. ChinaNANO 2017, Beijing, China, “Crystal Engineering with DNA” (2017).
147. Small Sciences Symposium, Beijing, China, “Next Generation Materials through Combinatorial Nanoscience” (2017).
148. ACS Publications Forum, Beijing China, “Ushering in The Digital Drug Design Revolution with Spherical Nucleic Acids” (2017).

The Jang Group

1. Lee, S.-H.; Jang, J.-W. MARCH 2017 Meeting of The American Physical Society, New Orleans, LA U.S.; “Semiconductor type dependent role of metal nanoparticle in metal and semiconductor nanostructured junction” (2017).
2. Lee, S.-H.; Hwang, S.; Jeong, J. H.; Jang, J.-W. MARCH 2017 Meeting of The American Physical Society, New Orleans, LA U.S.; “Abnormal behaviors in galvanically displaced Au nanostructure on silicon below and above percolation threshold a coverage of Au nanostructure” (2017).
3. Jang, J.-W. 2016 Fall Meeting of the Korean Physical Society, Gwangju, Korea; “Semiconductor type dependent role of metal nanoparticle in metal/semiconductor nanostructured junction” (2016).
4. Jang. J.-W. Young Giants of Nanoscience 2016, Hongkong, China; “Investigation on metal nanostructure/semiconductor junction and its applications” (2016).
5. Lee, S.-H.; Jang, J.-W. MARCH 2016 Meeting of The American Physical Society, Baltimore, MA U.S.; “Improvement of polypyrrole nanowire devices by plasmonic space charge generation: high photocurrent and wide spectral response by Ag nanoparticle decoration” (2016).
6. Lee, S.-H.; Jang, J.-W. MARCH 2016 Meeting of The American Physical Society, Baltimore, MA U.S.; “Unconventional but tunable phase transition above the percolation threshold by two-layer conduction in electroless-deposited Au nanofeatures on silicon substrate” (2016).
7. Jang. J.-W. 2015 International Chemical Congress of Pacific Basin Societies, Honolulu, HI U.S.; “Controllable metal-to-insulator transition in electroless-deposited Au nanofeatures on sillicon substrate” (2015).
8. Jang. J.-W. Symposium of Korea-Taiwan Research for Nano Materials and Nano Fabrications, Busan, Korea; “Au Nanomembrane for Two-Tone Micro/Nanolithography” (2015).
9. Yang, M.-S.; Jang, J.-W. 2015 Fall Meeting of the Korean Physical Society, Gyeongju, Korea; “Control-factors for Colloidal Nanoparticle Assembly Fabrication on a Self-assembled Monolayer-patterned Substrate” (2015).
10. Lee, S.-H.; Jang, J.-W. 2015 Fall Meeting of the Korean Physical Society, Gyeongju, Korea; “Improvement of polypyrrole nanowire device by plasmonic space charge generation: high photocurrent and wide spectral response by Ag nanoparticle decoration” (2015).
11. Oh, C.-M.; Jang, J.-W. 2015 Fall Meeting of the Korean Physical Society, Gyeongju, Korea; “Gold Membrane as a Material for Two-Tone Nanolithography” (2015).
12. Yang, M.-S.; Park, B.; Moon, B. K.; Jang, J.-W. BIT's 4th Annual World Congress of Nano Science & Technology, Qingdao, China; “Fabrication of ZrO2 Nanoparticle Array Using Colloidal Assemble Method” (2014).
13. Lee, S.-H.; Oh, C. M.; Shin, M.; Hwang, S.; Jang, J.-W. BIT's 4th Annual World

Congress of Nano Science & Technology, Qingdao, China; “Tunable Phase Transition above the Percolation Threshold” (2014).

14. Jang, J.-W. International Conference on Advances in Materials Chemistry, Taipei, Taiwan; “Light-matter Interaction in Metal-semiconductor Nano Systems” (2014).
15. Jang, J.-W. IUMRS-ICEM, Taipei, Taiwan; “Nano/micro Features of Soft Materials by Tip-based Nanolithography” (2014).
16. Jang, J.-W. Photonics WEST, San Francisco, CA; “Array of Nano/Micro Polymer Lenses for Subwavelength Optical Lithography” (2014).

e) manuscripts submitted, but not yet published

Mirkin-Jang Collaboration

1. Lee, S.-H.; Lee, S. W.; Oh, T.; Petrosko, S. H.; Mirkin, C. A.; Jang, J.-W. “Direct observation of plasmon-induced interfacial charge separation in metal/semiconductor hybrid nanostructures by measuring surface potentials,” *under review*.

f) provide a list any interactions with industry or with Air Force Research Laboratory scientists or significant collaborations that resulted from this work.

- This work in part led to the Center of Excellence for Advanced Bioprogrammable Nanomaterials (C-ABN), Northwestern-AFRL, FA8650-15-2-5518, June 2015-June 2020.
- The Mirkin group has published three papers with AFRL researchers:
    - Ashley, M. J.; Bourgeois, M. R.; Murthy, R. R.; Laramy, C. R.; Ross, M. B.; Naik, R. R.; Schatz, G. C.; Mirkin, C. A. “Shape and Size Control of Substrate-Grown Gold Nanoparticles for Surface-Enhanced Raman Spectroscopy Detection of Chemical Analytes,” *ACS Nano* **2017**, submitted.
    - Ross, M. B.; Ashley, M. J.; Schmucker, A. L.; Singamaneni, S.; Naik, R. R.; Schatz, G. C.; Mirkin, C. A. “Structure-Function Relationships For Surface-Enhanced Raman Spectroscopy-Active Plasmonic Paper,” *Journal of Physical Chemistry* **2016**, *120*, 20789-20797, doi: 10.1021/acs.jpcc.6b02019.
    - Schmucker, A. L.; Dickerson, M. B.; Rycenga, M.; Mangelson, B. F.; Brown, K. A.; Naik, R. R.; Mirkin, C. A. “Combined Chemical and Physical Encoding with Silk Fibroin-Embedded Nanostructures,” *Small* **2014**, *10*, 1485-1489, doi: 10.1002/smll.201302923.
- Mirkin gave a talk at the Air Force Research Laboratory Human Performance Seminar, Dayton, OH, “Profiling State of Health with Biomarkers Identified Based Upon Ultrahigh Sensitivity, Highly Multiplexed Assays” (2016).